Title

CHARACTERIZATION OF MULTICHANNEL SOURCES AND DESIGN OF MOLECULAR BEAM SYSTEMS FOR THEIR UTILIZATION

Authors

Jones, R.H.
Kruger, V.R.
Olander, D.R.

Publication Date

1968-10-01

UCRL-17859

eg 2

CHARACTERIZATION OF MULTICHANNEL SOURCES AND DESIGN OF MOLECULAR BEAM SYSTEMS FOR THEIR UTILIZATION

R. H. Jones, V. R. Kruger, and D. R. Olander

December 1968

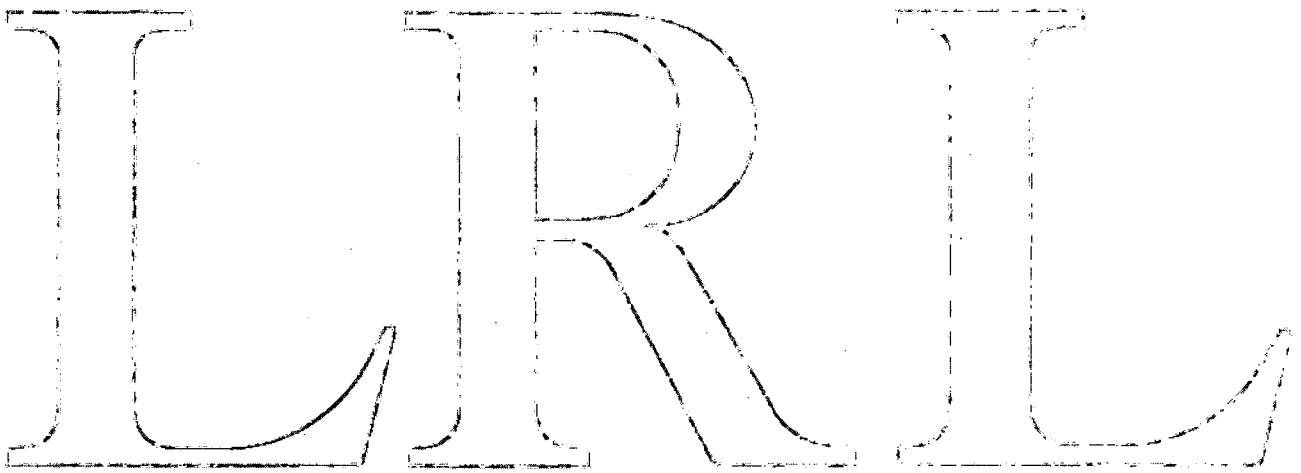

LAWRENCE RADIATION LABORATORY
UNIVERSITY of CALIFORNIA BERKELEY

eg 2

UCRL-17859

DISCLAIMER

UCRL-17859

UNIVERSITY OF CALIFORNIA

Lawrence Radiation Laboratory
Berkeley, California
AEC Contract No. W-7405-eng-48

CHARACTERIZATION OF MULTICHANNEL SOURCES AND DESIGN OF MOLECULAR BEAM SYSTEMS FOR THEIR UTILIZATION

R. H. Jones, V. R. Kruger, and D. R. Olander

December 1968

Printed in the United States of America
Available from
Clearinghouse for Federal Scientific and Technical Information
National Bureau of Standards, U. S. Department of Commerce
Springfield, Virginia 22151
Price: Printed Copy $3.00; Microfiche $0.65

TABLE OF CONTENTS

I. INTRODUCTION 1

(a) The Ideal Thin-Walled Orifice Source 3

(b) Channel Sources 5

(c) Optimum Source Configuration 13

II. EXPERIMENTAL 16

(a) Total Leak Rate 17

(b) Peaking Factor 18

(c) Signal-to-Background Ratio 18

III. RESULTS 19

(a) Single Capillary Source 19

(b) Krinkly Foil Source 22

(c) Quartz Membrane Source 23

(d) Mosaic Sources 24

IV. DISCUSSION 25

Appendix A 29

Appendix B 32

Appendix C 36

Appendix D 40

Notation 44

References 46

CHARACTERIZATION OF MULTICHANNEL SOURCES AND DESIGN OF MOLECULAR BEAM SYSTEMS FOR THEIR UTILIZATION

R. H. Jones, V. R. Kruger, and D. R. Olander

Inorganic Materials Research Division, Lawrence Radiation Laboratory,
Department of Nuclear Engineering, College of Engineering
University of California, Berkeley, California

ABSTRACT

An apparatus for measuring the leak rates and angular distributions of the molecular flux from multichannel sources was constructed. Four types of beam sources were tested: a single capillary, a Krinkly foil stack, an electron beam milled quartz membrane, and two sources constructed by fiber optics techniques (Mosaic sources).

The leak rates of the sources were compared to the predictions of Knudsen flow. The conductances of the Mosaic sources were 30-60% smaller than expected, possibly because of blockage of some of the channels. The conductances of the quartz membrane and Krinkly foil sources were considerably greater than the values predicted by Knudsen flow indicating the presence of leakage paths other than the observed channels. The conductance of the single capillary source was close to theory.

The angular distributions were characterized by a "peaking factor," defined as the ratio of the center-line beam intensity from the source to that from a cosine emitter of the same total flow rate. A semi-empirical formula was developed to correlate the peaking factors with the source pressure and Clausing factor of the channels. The correlation contained three terms: a molecular flow contribution derived by modification of the long tube Giordmaine-Wang calculation for short tubes; an empirical

slip flow term; and a viscous flow term chosen to approach the peaking factor predicted from isentropic flow theory at high source pressures. All measured peaking factors, except for that from the Krinkly foil source, adequately fit the correlation.

I. Introduction

In recent years there have been numerous studies of the interaction of molecular beams of non-condensable gases with solid surfaces. Datz et al. (1) and Smith and Fite (2) have investigated the scattering of helium and hydrogen from platinum and tungsten surfaces. Krakowski (3) has studied the dissociation of hydrogen on tantalum, and Steele (4) has investigated the reaction of oxygen and tungsten.

The primary difficulty with experiments of this type is the low intensity of the molecular beams, which necessitates sophisticated techniques for achieving a usable signal-to-noise ratio. The equivalent pressure of the beams (in terms of rate of impingement on the solid target) is typically on the order of 10^{-5} torr or less. Problems of beam intensity and beam formation have been reviewed by Pauly and Toennies (5) and by Anderson et al. (6).

A typical experimental arrangement by which a molecular beam is formed and directed at a target is shown in Fig. 1. The source tube contains a non-condensable gas at a pressure of p_s torr. At one end of the source tube is an aperture or multichannel array through which the gas in the source tube escapes into the source chamber by hydrodynamic and/or Knudsen flow. The source chamber is maintained at a low pressure p_o by a vacuum pump of speed S_o. The gas emission from the tip of the source tube is characterized by a total leak rate ℓ molecules/sec and an angular emission pattern $J(\theta)$ molecules/sec-steradian at polar angle θ. The flow pattern depends upon the source pressure and the geometry of the aperture at the tip of the source tube. Generally, the pressure in the source chamber is low enough that back movement of the gas from the source chamber into the source tube can be neglected.

Less than 1% of the emitted molecules pass through the collimating orifice and become the "molecular beam". The intensity of the beam can be varied by adjustment of the source tube pressure, and the temperature of the beam can be controlled by suitable heating of the end of the source tube. The largest portion of the beam molecules must come directly from the source tube and not from the background gas in the source chamber. This is essential since the beam molecules may be dissociated, at an elevated temperature, or otherwise possess properties that would be modified by wall collisions. To minimize the flow of non-directed gas through the collimating orifice, the source chamber pressure should be as low as possible. The collimator size is sufficiently small to permit differential pumping between the two chambers, and pressure differences of 3 orders of magnitude are achievable.

The source chamber pressure is related to the leak rate and pump speed by,

$$\ell = 3.24\times10^{19}\, p_o\, S_o, \text{ molecules/sec} \qquad (1)$$

where p_o is in torr and S_o is in lit/sec. The numerical constant in Eq. (1) is 1/RT (in units of molecules/liter-torr), where R is the gas constant and T = 300°K. The small fraction of the total leak rate which passes through the collimator has been neglected in determining the gas load on the source chamber. It is generally desirable to keep the source chamber pressure at 10^{-4} torr or less, and a typical source chamber pump has a nominal speed of 500 liters/sec (a 6" oil diffusion pump with gate valve and cold trap). With these figures the "maximum permissable leak rate" from the source is approximately 2×10^{18} molecules/sec. It is often not practical to supply more pumping speed to the source chamber.

There is an abrupt increase in cost and size of a 10" oil diffusion pump over a six inch model. Also, the larger pump must be placed farther from the source chamber thereby increasing conductance losses between the source tube region and the pump unless an inconveniently large and expensive source chamber is used. The major flow restriction in the source chamber is generally at the crowded end where the source emits its gas load, and a larger pump may only marginally improve the net pumping speed.

The objective of the beam source is to attain as high a centerline beam intensity as possible without overloading the pump in the source chamber. This requires that the angular emission pattern $J(\theta)$ be as peaked as possible in the forward direction ($\theta=0$), and that the gross area of the source be small enough to be approximated as a point source.

(a) The Ideal Thin-Walled Orifice Source

This source consists of an orifice whose length is much smaller than its radius. The condition for pure Knudsen flow from such an orifice is that the mean free path, as determined by the source pressure, be greater than the orifice diameter. Under this condition the leak rate (ℓ^*, molecules/sec) is given by

$$\ell^* = \frac{p_s A}{\sqrt{2\pi mkT}} \qquad (2)$$

or, in more convenient units, by:

$$\ell^* = \frac{3.51\times10^{22}}{\sqrt{MT}}\, p_s A \qquad (3)$$

In Eq. (3) p_s is the source pressure (torr), A is the area of the orifice (cm^2), M is the molecular weight of the effusing gas, and T is the absolute temperature (°K).

In a gas at temperature T and pressure p_s the mean free path, λ, is determined by

$$\lambda = \frac{kT}{\sqrt{2}\,\pi\, p_s \sigma^2} = \frac{B}{P_s} \qquad (4)$$

where σ is the kinetic theory collision diameter of the gas molecule. At room temperature B of Eq. (4) is 5×10^{-3} cm-torr for air, and 1.5×10^{-2} cm-torr for helium.

Consider air at room temperature effusing through a single circular orifice of radius a under the limiting Knudsen condition $\lambda = 2a$. Combination of Eqs. (3) and (4) shows that $\ell^* = 2.8\times10^{18}a$. Thus, to achieve the "maximum permissible" leak rate of 2×10^{18} molecules/sec, a 2 cm diameter hole would be required. After collimation by an aperture of (typically) 1mm diameter downstream of the source, the usable beam intensity at the target would be disastrously smaller than that from a true point source of the same strength. To be considered a point source (for this example) the aperture should be about 1mm diameter. However, a 1mm orifice at the Knudsen flow limit yields a leak rate of 1.4×10^{17} molecules/sec, an order of magnitude below the maximum leak rate set by the allowable chamber pressure. Thus, the dual requirements of small source size and maximum leak rate cannot be met by an ideal circular orifice.

Ribbon shaped beams from slit sources operated in Knudsen flow can deliver the "maximum leak rate". The mean free path consideration applies to the slit width, and the slit length may be made sufficient

to obtain the necessary flow. Alignment problems associated with ribbon beams and the strip geometry of targets and detectors place slits sources in a class by themselves and slit sources will not be considered here. Only circular, axially symmetric sources will be discussed.

The angular distribution of the molecules emitted from an ideal thin-walled source is

$$J(\theta) = \ell^* \frac{\cos\theta}{\pi} \tag{5}$$

and the centerline intensity is

$$J(0) = \frac{\ell^*}{\pi} \tag{6}$$

The solid angle subtended by the collimator of radius r_1 cm separated from the emitting orifice by d cm is $\pi(r_1/d)^2$ steradian. The fraction of the emitted molecules which pass through the collimating orifice is $(r_1/d)^2$. For r_1 = 0.05 cm, d = 1.5 cm, 0.1% of the emitted molecules contribute to the collimated molecular beam. The maximum permissible air leak rate from a 1mm diameter source aperture under the limiting Knudsen condition $\lambda = 2a$ is 1.4×10^{17} molecules/sec. Using this figure in Eq. (6) yields a centerline intensity of 5×10^{16} molecules/sec-cm^2. For a target placed 10 cm from the source, the beam strength is only 5×10^{14} molecules/sec, or an equivalent pressure of 3×10^{-7} torr. Molecular beams of this intensity are too weak for many experiments. In addition, the capacity of the pump on the source chamber (which is assumed to be capable of handling a flow of $\sim 2\times10^{18}$ molecules/sec) is not utilized.

(b) Channel Sources

In order to increase the centerline beam intensity above that of an

ideal circular orifice, the source tip can be made up of many long, small bore channels or capillaries, each emitting independently. The angular emission pattern from this type of source is more peaked than that from a thin-walled orifice, and therefore the number of molecules contributing to the beam can be increased without increasing the total flow rate. The restriction that the bundle of channels have a gross area small enough to be considered as a point source must still be considered (i.e., overall diameter $\sim$ 1mm).

The leak rate from a single long channel of radius a and length L can be written as

$$\ell = K\ell^* F(p_s/p^*) \tag{7}$$

where K is the Clausing factor

$$K = (1 + \frac{3}{8}\frac{L}{a})^{-1} \tag{8}$$

and p^* is the source pressure at which the mean free path is equal to the tube diameter

$$p^* = \frac{B}{2a} \tag{9}$$

ℓ^* is the leak rate through an ideal thin-walled orifice of area $A = \pi a^2$, as given by Eq. (2) or (3).

The factor $F(p_s/p^*)$ has the following limits: at low source pressure the flow is entirely in the Knudsen regime

$$F \to 1 \text{ as } (p_s/p^*) \to 0 \tag{10}$$

the leak rate at high source pressures is given by the Poiseuille formula with the viscosity given by elementary kinetic theory [$\mu = (mkT)^{1/2}/\pi^{3/2}\sigma^2$]:

$$F \to \frac{3\pi}{256}\left(\frac{p_s}{p^*}\right) \text{ as } (p_s/p^*) \to \infty \tag{11}$$

Fryer (7) has developed a formula for $F(p_s/p^*)$ which has these limits and agrees with Knudsen's experimental measurements at intermediate pressures. For the leak rate he obtains, in terms of pressure and pressure

gradient

$$\ell = \frac{4}{3} a^3 \left(\frac{2\pi}{mkT} \right)^{1/2} \left\{ \frac{p^*}{p + p^*} + \frac{\pi}{4} \frac{p}{p + p^*} + \frac{3\pi}{128} \left(\frac{p}{p^*} \right) \left[1 - g\left(\frac{p}{p^*} \right) \right] \right\} \frac{dp}{dz}$$

The first term in the brackets represents Knudsen flow, the second slip flow, and the third Poiseuille flow with the low pressure correction given by Scott and Dullien (13) as

$$g\left(\frac{p}{p^*} \right) = -\left(\frac{p}{p^*} \right) + \left[\left(\frac{p}{p^*} \right)^2 + 1 \right]^{1/2}$$

As shown in Appendix A, integrating from $p=p_s$ at $z=L$ to $p=0$ at $z=0$ and writing the results in the form of Eq. (7) yields

$$F\left(\frac{p_s}{p^*} \right) = \frac{1}{(p_s/p^*)} \left\{ \frac{\pi}{4} \left(\frac{p_s}{p^*} \right) + \left(1 - \frac{\pi}{4} \right) \ell n \left(\frac{p_s}{p^*} + 1 \right) \right.$$

$$\left. + \frac{\pi}{128} \left[\frac{3}{2} \left(\frac{p_s}{p^*} \right)^2 + \left(\frac{p_s}{p^*} \right)^3 - \left(\left(\frac{p_s}{p^*} \right)^2 + 1 \right)^{3/2} + 1 \right] \right\} \quad (12)$$

This equation is plotted in Fig. 2.

The Knudsen expression (F=1) predicts the flow rate to within 10% up to $p_s/p^* = 10$. Effusive beam sources are always operated at $p_s/p^*<10$. While $\ell=K\ell^*$ predicts the correct flow up to $p_s/p^*=10$, this does not imply that pure Knudsen flow exists up to this pressure. The fraction of total flow in each flow regime can be determined from the integrated form of Fryer's equation (Appendix A). The results of this determination are shown in Fig. 3.

The angular emission characteristics of a long channel can be most conveniently expressed by the ratio of the centerline intensity from the channel source to the centerline intensity from an ideal thin-walled source emitting at the same total leak rate. A "peaking factor" (or "directivity") is defined by

$$\chi \equiv \frac{[J(0)]_\ell}{[J^*(0)]_\ell} = \frac{\pi}{\ell} [J(0)]_\ell \tag{13}$$

Since for an axially symmetric source ℓ can be written as

$$\ell = 2\pi \int_0^1 J(\theta)\, d\,(\cos\theta) \tag{14}$$

the peaking factor is

$$\chi = \frac{J(0)}{2\int_0^1 J(\theta)\, d(\cos\theta)} \tag{15}$$

For channels in which the upstream pressure is low enough such that $\lambda > L$ (more restrictive than the Knudsen condition for total flow, $\lambda > 2a$), the centerline intensity is due only to those molecules which pass through the tube without collisions (wall or intermolecular). In this case the centerline intensity is the same as that from an ideal thin-walled orifice of radius a, but the total flow rate is the product of the Clausing factor and the ideal orifice leak rate.† The maximum peaking factor for a

† If ℓ^* is the leak rate which would occur through a thin-walled orifice of radius a, it is also the rate at which molecules enter the channel at the high pressure end. Because of wall collisions only a fraction K of the ℓ^* molecules which enter the channel actually leak out, i.e., the channel leak rate is $K\ell^*$. However, the centerline intensity is unaffected by the presence of the walls and is given by ℓ^*/π.

channel is

$$\chi_{max} = 1/K \tag{16}$$

For example, the maximum peaking factor for a 0.63 cm long channel 0.038 cm in diameter is 14. However, if the mean free path is to be greater than the channel length, the total leak rate from one channel is only 3×10^{15} molecules/sec since the source pressure is limited to 8×10^{-3} torr (air). If there are N channels in the assembly, the flow is N times as great

$$\ell_{(N)} = N\ell_{(1)} \tag{17}$$

Therefore sufficient holes may be used to attain the "maximum permissable leak rate" of 2×10^{18} molecules/sec. However, 600 such holes would be required, and they would cover at least a 10mm diameter circle thereby violating the point source condition.

Two avenues of approach are open to increase the total leak rate, yet not entirely lose the favorable directional characteristics. One is to make the whole capillary smaller; the other is to operate at higher source pressures, thus suffering some attenuation of the centerline flux by intermolecular collisions.

When the upstream pressure is such that the entire length of the tube is not transparent to the gas molecules, $\lambda<L$, part of the flow in the tube is in the hydrodynamic flow regime. An estimation of the peaking factor for this case may be derived from the calculation of Giordmaine and Wang (8) which applies to the case of $L>>$ a (long tubes). Their result is:

$$\chi_{GW} = \left[\frac{3\pi}{8K}\left(\frac{p^*}{p_s}\right)\right]^{1/2} \operatorname{erf}\left[\frac{2}{3K}\left(\frac{p_s}{p^*}\right)^{1/2}\right] \tag{18a}$$

where $K = 8a/3L$.

A simplified form of Eq. (18a) valid when the source is opaque ($\lambda \ll L$, or the erf term is unity) is:

$$\chi_{GW} = \left[\frac{3\pi}{8K}\left(\frac{p^*}{p_s}\right)\right]^{1/2} \tag{18b}$$

For short tubes, a better fit to the data is obtained by using a peaking factor derived by the Giordmaine and Wang method but using a more realistic expression for the pressure in the channel and employing the short tube Clausing factor [Eq. (8)]. This peaking factor is derived in Appendix C for a general linear number density dependence and the result using the end conditions derived in Appendix B is

$$\chi = \frac{\alpha}{K\beta} + \frac{1}{K}\left[1 - \frac{\alpha + \frac{8}{3}\left(\frac{1}{K} - 1\right)}{\beta}\right]\exp\left\{-\frac{4}{3}\left(\frac{1}{K} - 1\right)\left[\alpha + \frac{4}{3}\left(\frac{1}{K} - 1\right)\right]\frac{(p_s/p^*)}{\beta}\right\}$$
$$+ \frac{1}{K}\left(\frac{\pi}{\beta}\right)^{1/2}\frac{\exp\left[\left(\frac{p_s}{p^*}\right)\left(\frac{\alpha^2}{4\beta}\right)\right]}{(p_s/p^*)^{1/2}}\left\{\operatorname{erf}\left[\left(\frac{p_s}{p^*}\right)^{1/2}\frac{\alpha + \frac{8}{3}\left(\frac{1}{K} - 1\right)}{2\beta^{1/2}}\right] - \operatorname{erf}\left[\left(\frac{p_s}{p^*}\right)^{1/2}\frac{\alpha}{2\beta^{1/2}}\right]\right\} \tag{19}$$

where

$$\beta = \frac{32}{3}\left(\frac{1-K}{K^2}\right)\left[\frac{1}{\bar{\mu}_L} - \frac{1}{\bar{\mu}_0}\right]^{-1}$$

$$\alpha = \beta K/4\bar{\mu}_0$$

and $\bar{\mu}_L$ and $\bar{\mu}_0$ are the average cosines of the angular distribution of the flux at the upstream and downstream ends of the channel, respectively.

The average cosine of the flux from the low pressure end has been determined empirically from the angular distribution measurements.

These patterns yield a value of $\bar{\mu}_0 = 0.7 \pm 0.02$ for all sources investigated. In view of the wide variety of sources tested, this invariance suggests that a value of 0.7 can be safely used for all multichannel sources.

Values of $\bar{\mu}_L$ for the extreme cases of very long tubes and very short tubes (i.e., a thin-walled orifice) can be inferred from the following considerations. For an isotropic gas the average cosine is zero. The deviation of the angular distribution of the flux at the inlet end of a tube is due to the perturbation caused by the net flow down the tube. For a very long tube, the net flow is small, so that the angular distribution at the inlet should be nearly isotropic, or $\bar{\mu}_L \to 0$ as $(L/a) \to \infty$ (or $K \to 0$).

For a thin-walled orifice emitting into a vacuum, all molecular trajectories are from the resevoir towards the vacuum, and the average cosine of the flux in the orifice is that of a cosine source, or $\bar{\mu}_L \to 2/3$ as $(L/a) \to 0$ (or $K \to 1$).

For tubes for which $L/a > 1$, a calculation based upon the same approximations inherent in the form of the Clausing factor given by Eq. (8) yields: (see Appendix B)

$$\bar{\mu}_L = \frac{1}{4} \frac{K}{1-K}$$

This formula approaches the proper limit as $K \to 0$ (long tube) but, because of the approximations in the derivation, does not exhibit the correct limit as $K \to 1$. Since the maximum value of $\bar{\mu}_L$ is 0.67, the above expression is valid only when the calculated $\bar{\mu}_L$ is considerably less than 0.67. The maximum Clausing factor for the sources tested here was 0.31, which corresponds to a maximum $\bar{\mu}_L$ of 0.11. This is well within

the range in which the approximate formula is applicable.

Equation (19) applies only in the low-pressure Knudsen region and cannot be expected to describe the experimentally determined peaking factor when a substantial amount of the flow is in the slip or viscous regime. As is evident from Fig. 3, even for values of (p_s/p^*) as low as 0.1, approximately 4% of the total flow is due to slip flow, and at $(p_s/p^*)=10$, the fraction in Knudsen flow is less than either the slip or viscous contributions. It is clearly desirable to make some correction to the theory at high pressures, so that a more meaningful prediction of the experimental results can be made.

Sibulkin and Gallaher (9) have derived an expression for the peaking factor for the case of pure viscous flow of a monatomic gas in a uniform duct, which results in $\chi = .976$, essentially independent of pressure. The high pressure limit of Eq. (19) is $1/(4\bar{\mu}_0) = 0.356$. This would suggest an additive correction term that approaches 0.976 - 0.356 = 0.62 in pure viscous flow. To accomplish this the following term is added to Eq. (19) to correct for the viscous contribution:

$$\chi_{vis} = 0.62 \; f_1(p_s/p^*) \tag{20}$$

where $f_1(p_s/p^*)$ is the fraction of total flow in the viscous regime, as computed from the integrated Fryer expression, (Fig. 3).

This correction will not account for the contribution due to slip flow, and since no theoretical expression is available for the peaking factor in that case, the following empirical correction is postulated:

$$\chi_{slip} = C \; f_2(p_s/p^*) \tag{21}$$

where $f_2(p_s/p^*)$ is the fraction of total flow in the slip regime (Fig. 3).

The corrected peaking factor will be given by:

$$\chi_{corr} = \chi_{mol} + \chi_{slip} + \chi_{vis} \qquad (22)$$

where χ_{mol} is given by Eq. (14).

The numerical coefficient C in Eq. (21) was determined by fitting the data (χ vs p_s/p^*) from one source to Eq. (22). A value C = 2.7 was obtained by this fit and applied without modification to all sources tested in this study.

(c) Optimum Source Configuration

The total source flow rate and the total source area $A = \pi r_s^2$ are determined by considerations not associated with the construction of the source tube. The maximum leak rate depends on the speed of the pump on the source chamber, and the gross radius of the source is limited by the point source condition. With these restrictions, the most efficient source is the one which gives the largest centerline flux for a given total flow rate:

$$J(0) = \chi N \frac{\ell(1)}{\pi} = \chi \frac{\ell}{\pi} = \text{maximum} \qquad (24)$$

Since the maximum value of ℓ is fixed by the capacity of the source chamber pump, the largest centerline intensity is attained with the source having the largest χ. Using Eqs. (3) (with $A=\pi a^2$), (7) (with F=1), (9) and (17), the total leak rate can be written as

$$\ell = \frac{3.5\times10^{22}\ \pi B}{2\sqrt{MT}} \left(\frac{p_s}{p^*}\right) KNa \qquad (25)$$

The transmissivity of the source is

$$\tau = \frac{N\pi a^2}{\pi r_s^2} = \frac{Na^2}{r_s^2} \tag{26}$$

Eliminating N between Eqs. (25) and (26) yields

$$K\left(\frac{p_s}{p^*}\right) = \frac{(a/\tau)}{\eta} \tag{27}$$

where

$$\eta = \frac{3.51\times10^{22}}{2\sqrt{MT}}\left(\frac{\pi r_s^2}{\ell}\right) B \tag{28}$$

According to Eq. (18b), the peaking factor is largest when the left hand side of Eq. (27) is smallest. The parameter η of Eq. (28) is independent of the details of source construction; it depends on the nature of the gas through M and B and on the maximum allowable source area and total source leak rate. To maximize the centerline beam intensity, the ratio τ/a (which is Hanes' (10) figure of merit of a source) should be as large as possible. This requires highly transparent sources with small radius channels.

Table 1 lists the various types of multichannel sources which have been studied by previous investigators. Source D, the Zacharias Krinkly foil source, has been used most extensively in experiments where hot beams are required, since it can be constructed entirely out of a refractory metal. Source G is theoretically the most efficient, but because of the plastic used in its construction, cannot be used at elevated temperatures. The variation of the peaking factor with reduced pressure for source A is shown on Fig 4, along with the theoretical curves represented by Eqs. (18), (19) and (22).

Table 1 - Characteristics of Various Multichannel Sources*

	Source Type	Channel length, L, cm	Effective radius of channel, a, cm	No. of Channels per 10^{-2} cm^2	Clausing factor of Channels K	Transmissivity of Source, τ	$\frac{\tau}{a}$
A	extended klystron grid structure, individual hexagonal shaped channels separated by walls ~0.001 in. thick	0.66	1.65×10^{-2}	11	0.067	0.44	7.6
B	aligned stack of photographically etched metal foils, circular holes on hexagonal pattern	0.31	2.35×10^{-3}	96	0.020	0.15	7.9
C	Nickel Krinkly foil, rolled onto thin spindle - Triangular shaped channels	0.95	2.69×10^{-3}	190	0.0076	0.27	10.0
D	Original Zacharias Krinkly foil	0.66	3.8×10^{-3}	110	0.0153	0.50	11.5
E	5 mil Klystron grid tubes	0.38	5.9×10^{-3}	81	0.041	0.85	12.0
F	1 mil Klystron grid tubes	0.026	1.27×10^{-3}	530	0.13	0.27	14.6
G	#46 enameled copper wires embedded in epoxy and then electrolytically removed	0.063	1.97×10^{-3}	530	0.083	0.65	18.2

* From Giordmaine and Wang (8) and Hanes (10)

UCRL-17859

II. Experimental

The apparatus used to measure the angular distribution from sources is similar to that of Giordmaine and Wang (8), Hanes (10), and Johnson et al. (11). Photographs of the device are shown in Figs. 5 and 6, and a schematic in Fig. 7. A six inch stainless steel tee pumped by a six inch oil diffusion pump houses the source to be tested and the gas sampling probe. The probe may be positioned at angles up to 55° each side of the source tube axis. The probe tip is a capillary 1/4" long formed by a No. 80 drill (K=1/14). The capillary tip reduces the response to the directed emission by 19% (Appendix D), but further reduces the background contribution by the full Clausing factor of 1/14. The probe tip swings on a 5 cm radius about the tip of the source and thus intercepts an angle of 0.37°, providing excellent resolution.

The geometrical alignment may be specified as follows:

(a) The probe tip swings in a plane and the source axis is constrained to lie in that plane.

(b) The axis of probe rotation and the source axis intersect at the tip of the source.

To achieve proper alignment, a thrust bearing supports the probe a fixed distance above the source tip. The remaining degree of freedom, the cant of the source tube relative to the probe plane of swing, is adjusted by raising or lowering the rear coverplate through which the source tube passes, similar to the positioning of a billiard cue in the shooter's hands.

Alignment is achieved when a beam from a gas laser passes through a 1/32" diameter mock capillary source and through the probe at the straight ahead position. After alignment, the mock capillary is replaced by the source to be tested.

A beam flag is incorporated into the apparatus to permit readings of the gas background to be taken.

Following Hanes (10), helium was used as the test gas and the sampling probe was connected directly to a commercial helium leak detector. The pressure of helium in the source tube was measured on a Wallace-Tiernan absolute pressure gauge covering 0.1 to 20 torr, and on a thermocouple gauge in the range 10μ to 500μ. Both gauges were calibrated against a McLeod gauge using helium from 20μ to 5 torr.

(a) Total Leak Rate

The conductance of the source is related to the driving pressure and the leak rate by

$$\ell = 3.24\times10^{19}\, C_s p_s \qquad (29)$$

where the chamber pressure (p_o) has been neglected. C_s is the source conductance in lit/sec and p_s is in torr. For a source consisting of N uniform channels of radius a (cm) in Knudsen flow (or, according to Fig. 2, for $p_s/p^* < 10$), the conductance is

$$C_s = K\frac{3.51\times10^{22}}{3.24\times10^{19}}\frac{N\pi a^2}{\sqrt{MT}} = 98\, N\, K\, a^2 \qquad (30)$$

The last equality is for helium at 300°K.

The conductance of the source is determined by the rate of pressure decrease in the reservoir which supplies the source tube (24 lit). The rate at which the source pressure decreases with time is given by

$$\frac{p_s}{p_s^o} = \exp\left\{-\left(\frac{C_s}{V_r}\right)t\right\}$$

The source conductance can be determined from a semilog plot of source pressure versus time. C_s may be a function of p_s if the flow is not in the Knudsen regime during the entire transient pressure decay period.

(b) Peaking Factor

The apparatus is primarily designed to measure the factor χ in Eq. (15). Data on the leak detector response as a function of angle θ, denoted by $s(\theta)$, and the background signal, s_{bkg}, were obtained. Measurements up to $\theta = 55^\circ$ on either side of the axis were made. After subtraction of the background signal, the first flight flux down the probe is proportional to $J(\theta)$, and Eq. (15) becomes

$$\chi = \frac{s(0) - s_{bkg}}{\int_0^{\frac{\pi}{2}} [s(\theta) - s_{bkg}] \, d(\cos\theta)} \tag{31}$$

The denominator of Eq. (31) is computed by numerical integration of the experimental data. While hand computation is practical, our large collection data was processed by computer.

(c) Signal-to-Background Ratio

The ratio of the first flight signal along the centerline to the background signal is defined as the "signal-to-background ratio".

$$\rho = \frac{s(0) - s_{bkg}}{s_{bkg}} \tag{32}$$

In Appendix E it is shown that $\rho = \rho^*/\chi$ where $\rho^* = 2.3$ for the apparatus used in this study. By employing the beam flag, both $s(0)$ and s_{bkg} may be obtained and a check on the apparatus made by calculating ρ^*.

III. Results

Five sources of various types were tested in the apparatus of Fig. 7. The characteristics of these sources are shown in Table 2. The performance of each source is discussed in the sections which follow.

(a) Single Capillary Source

A single-capillary source was fabricated and tested in order to evaluate the performance of the apparatus. The pressure decay curve for this source is shown in Fig. 8. The experimental curve at high pressures is greater than the extrapolated straight line section. This curvature arises from the non-linear pressure dependence of the leak rate (i.e., $F > 1$), and occurs as expected for source pressures greater than 3.8 torr ($p_s/p^* > 10$).

A typical polar diagram of the angular distribution is shown on Fig. 9, along with a circle characteristic of a cosine emitter of the same strength. A summary of the peaking factors, and signal-to-background ratios is shown in Table 3.

The signal-to-background ratio ρ^* is constant to within 5% over a 100-fold source pressure variation. However, its value is 15% smaller than the predicted value of 2.3, (Appendix E), perhaps due to lower pumping speed than the estimated 500 lit/sec. For low pressures the background signal becomes very small and difficult to measure. Also any alignment errors become more important as the highly peaked angular distributions are difficult to measure at their highest point. Both these effects explain the increased scatter and falling off of the ρ/χ values at low pressures.

The peaking factor is plotted as a function of p_s/p^* in Fig. 10. The various theoretical curves are also graphed.

Table 2. Characteristics of Sources Investigated

Source	Radius of Single Channel (cm)	Channel Length (cm)	Gross Source Radius (cm)	No. of Channels (counted)	Transmissivity % (calculated)	Clausing Factor (K)	p^* (torr) helium	Source Conductance (lit/sec x 10^3) Calc.	Expt.
Single Capillary	0.019	0.478	0.019	1	100	0.096	0.38	3.4 1.3	3.0 (He) 1.5 (air)
Krinkly Foil	0.0038	0.60	0.078	104	25	0.017	1.9	2.5	52.0 (He)
Quartz Membrane	0.0050	0.030	0.05	70	38	0.31	1.46	7.6	25.6 (He)
Mosaic A	0.00055	0.025	0.050	4290	52	0.050	13.3	7.4 2.7	5.8 (He) 1.9 (air)
Mosaic B	0.0045	0.028	0.044	33	34	0.28	1.62	27.4 10.2	9.0 (He) 4.1 (air)

UCRL-17859

Table 3. Summary of Measurements on Single Capillary Source

p_s (torr)	χ	ρ	ρ/χ
3.04	2.8	6.1	2.1
2.01	3.2	7.0	2.4
1.49	3.4	7.3	2.0
1.06	3.9	8.0	2.1
0.85	4.1	9.1	2.0
0.70	4.4	9.5	2.1
0.48	4.7	9.7	2.0
0.30	5.9	10.8	1.8
0.19	6.4	12.6	1.9
0.11	6.8	12.8	1.9
0.050	8.4	13.3	1.5
0.040	8.8	13.2	1.4
0.018	11.4	8	0.7

(b) Krinkly Foil Source

The multichannel source shown in Fig. 11 was used by Krakowski (3) as a source of high temperature hydrogen beams. A circular array of approximately 100 channels with an overall source diameter of 1.5 mm was formed by alternately stacking flat and corrugated tantalum foils into a 3 mm slot milled into the end of a 1/2" tantalum rod. The 1.5 mm diameter hole connects the back of the foil stack to the gas supply tube.

The straight line portion of the pressure decay curve for this source indicated a conductance of 5.2×10^{-2} lit/sec, which is twenty times greater than that calculated from the geometry of the channels.

Angular distributions were measured with the slot containing the foil stack in the plane of swing of the probe (the horizontal arrangement) and at 90° to this plane (the vertical arrangement). A polar plot with the slot horizontal is shown in Fig. 12 and a distribution with slot vertical is shown in Fig. 13. The pear-shaped appearance of these curves indicates appreciable emission at large polar angles. The effect is more pronounced with the slot in the plane of the probe rotation (the horizontal arrangement) than with the slot vertical. The large discrepancy between the theoretical and calculated leak rates and the broad wings on the angular distributions suggests considerable leakage through the channels which were supposedly blocked and along the milled slot.

Peaking factors were calculated for the vertical and horizontal measurements independently and ignoring the observed axial asymmetry. A comparison of the experimental peaking factors with theory is shown in Fig. 14. The large discrepancy between the experimental and theoretical peaking factors confirms the existence of appreciable gas leakage from

parts of the source assembly other than the central channels. The vertical slot traverse misses some of the emission from off-center channels of the foil stack which were supposedly blocked. Therefore, the angular distributions are narrower and yield higher peaking factors for the vertical slot arrangement than with the slot horizontal. Scott (12) found that a stacked foil source did not yield peaking factors as high as predicted by theory, even when all observable extraneous leakage paths had been closed.

(c) Quartz Membrane Source

A source consisting of channels formed in a quartz membrane was produced by electron beam milling.* A photograph of the channel array is shown in Fig. 15. The source had non-uniform holes, some larger than 100 microns diameter. In counting the number of channels for a theoretical leak rate determination, only the obvious holes in Fig. 15 were included. The non descript region at the bottom of the photograph is due to fingers of quartz which solidified from the molten material ejected during the EB drilling. There are undoubtedly open channels obscured by the resolidified quartz, but no attempt was made to estimate their size or number. Thus, the calculated conductance is considerably smaller than the observed value. The leak rate and peaking factor results are shown in Figs. 16 and 17. Although this source delivers only modest peaking factors, it can be used at temperatures up to 1200°C even with gases which would rapidly attack metals.

* Electron beam milling was done by TRI-D Corporation, 7 Johnson Avenue, Plainville, Connecticut 06062.

(d) Mosaic Sources

Two multichannel sources composed of many glass tubes bunched together were fabricated from thin sections of fiber optics material.* Photographs of each channel array are shown in Figs. 18 and 19. While the soft glass and sealant used in their construction limit the use of these sources to temperatures below 450°C, their potentially large peaking factors make them very attractive for low temperature applications.

The helium leak-down plots are shown in Figs. 20 and 21. A typical highly peaked angular distribution (χ = 12.6) from source A is shown in Fig. 22. The variation of the peaking factors with source pressure is shown in Figs. 23 and 24.

* The fiber optics material was sliced and sealed to the ends of glass tubes by Bendix Mosaic Fabrications, Sturbridge, Massachusetts.

IV. Discussion

The leak rate (or conductance) measurements have been reported for the linear portions of the pressure decay curves and are theoretically described by Eq. (30). Only the single capillary source is in reasonable agreement with this formula; the helium conductance is 12% below the theoretical value and the air leak rate is 15% greater than Eq. (30). The leak rate from the Krinkly foil source includes the very large contribution due to leakage from the base of the foil stack. Determination of the number of holes in the quartz membrane source is too difficult to predict an accurate theoretical conductance. The geometry and number of holes in the Mosaic sources, however, are well defined, but the measured conductances are 25 and 65% smaller than the Knudsen flow predictions for sources A and B respectively.

The ratio of the experimental conductances for helium and air is 2.0 for the single capillary and 3.0 and 2.2 for Mosaic sources A and B respectively. The theoretical value for Knudsen flow is 2.7. If the probable error on C_s is taken as $\sim \pm 15\%$ (as determined from the single capillary source measurements), the error in the ratio $(C_s)_{He}/(C_s)$ air should be $\sim \pm 21\%$. By this criterion, the helium-to-air conductance ratios for the two Mosaic sources are in accord with the square root of the molecular weight prediction of molecular flow.

The various theoretical peaking factor formulae against which the data have been compared all yield the same predictions at reduced source pressures of 0.2 - 0.5. At lower pressures, the peaking factors should

approach the Knudsen limit of 1/K. The simplified Giordmaine and Wang expression (Eq. (18b)) does not have this limit. The full Giordmaine and Wang expression (Eq. (18a)) approaches the proper limit, but the Clausing factor is that appropriate for long tubes. For the short channel sources, the expression used for the Clausing factor is important, as seen from the theoretical curves on Figs. 17 and 24. Experimentally, the approach of the peaking factor to the Knudsen limit is evident from Figs. 10 and 23.

In many molecular beam applications, short tube (or small L/a) sources operated at high reduced source pressures are required to produce sufficiently intense beams and fully utilize the capacity of the source chamber pump. In this instance, the peaking factors measured for the quartz membrane and Mosaic B sources would be typical for the above experimental conditions. None of the theoretical formulae based upon molecular flow reveal the unexpectedly high peaking factors observed for these sources. However, the correction factors accounting for the contributions of slip and viscous flow adequately reproduce the data for all sources, even though the coefficient of Eq. (21) was determined from the Mosaic B source data.

The correlation applies only to helium which was used in all angular distribution measurements. The molecular flow component given by Eq. (19) can be applied to other gases by use of the proper $\bar{p}^*$. The numerical coefficient in Eq. (20) is determined by the high pressure limit of the peaking factor from isentropic flow theory, and depends upon the specific heat ratio of the gas (9). The dependence of the empirical coefficient of Eq. (21) upon the type of gas, however, is not known. In the region of reduced source pressures ~ 5, the slip flow term accounts for the bulk of the peaking factor. Additional work is needed to determine

the effect of the gas on this coefficient before Eqs. (19) and (22) can be used for design purposes at high source pressures. At reduced source pressures less than unity, the molecular flow term predominates and the formulation can be used for any gas.

Of all the data reported here, only the conductances of the Mosaic sources are in sizable disagreement with theory. The angular distributions from these two sources, however, fit the correlation which applies to the other sources. If the empirical slip flow contribution to χ is minimized by low pressure operation, the peaking factors from the Mosaic sources approach the theoretically sound value of 1/K (see Figs. 23 and 24). Yet in the same source pressure range, the conductances were 25 to 65% lower than that expected by Knudsen flow. The theoretical peaking factors depend only upon the flow characteristics of a single channel, and the total leak rate is eliminated from the experimental values by the ratio of Eq. (15). This implies that the flow in the individual channels of the Mosaic sources is behaving according to theory, but that only a fraction of the channels are open. Although the photographs of the Mosaic sources (Figs. 18 and 19) do not reveal a substantial number of blocked channels, the likely material which would be blocking the flow passages is transparent (i.e., glass or the binder used in fabrication). Thus many channels could be blocked and the reduced flow area may not be visible from photographs of the array.

Stickney et al. (14) have measured the angular distribution of cesium vapor from tubes having length-to-diameter ratios of 0.04 to 5.63. Reduced pressures (or inverse Knudsen numbers) from 0.01 to 5 were investigated. Because the slit shaped surface ionization detector had a rather substantial angular resolution ($\pm 4^\circ$), the maximum peaking factors of Eq. (16) were

not attained, even at the lowest source pressures*. Figs. 9 and 22 show the pointed character of the angular distributions at low source pressures. The maxima of the carrot-shaped curves typified by Fig. 22 are very difficult to measure; very careful alignment and good angular resolution are needed.

We did not observe minima in any of the peaking factor plots, as did Stickney et al. for reduced pressures between one and five. These minima may be connected with the augmentation of the total flow by surface diffusion along the channel wall. The effect of surface diffusion on molecular beams from effusion ovens has been considered by Winterbottom (15). In the cesium beam oven used by Stickney et al., higher source pressures are achieved by increasing the temperature of the oven and super-heater. Hence surface diffusion would be most significant for their high source pressure experiments. However, our experiments do not clearly eliminate the possibility of minima in the peaking factors for permanent gases, since we do not have sufficiently extensive data for short tubes at high pressures, where the effect appears to be most pronounced.

Acknowledgement - This work was supported by the United States Atomic Energy Commission.

---

* Fig. 9 of ref. 14 is analogous to the peaking factor plots presented here. The abcissas are identical, but the ordinate in Fig. 9 of ref. 14 is equivalent to χ/χ_{max} instead of the χ used in our plots.

APPENDIX A - Derivation of $F(p_s/p^*)$

The expression for $g(p/p^*)$ given by Scott and Dullien (13) is:

$$g(p/p^*) = \exp[-\sinh^{-1}(p/p^*)] \tag{A-1}$$

A more tractable expression for $g(p/p^*)$ can be obtained as follows:

$$\text{Since} \quad \sinh x \equiv \frac{e^x - e^{-x}}{2} = \frac{p}{p^*}$$

Then $\sinh^{-1}(p/p^*) = x$, and $g(p/p^*) = e^{-x}$. Therefore, from the definition of sinh x,

$$e^x - e^{-x} = \frac{1}{g(p/p^*)} - g(p/p^*) = 2(p/p^*)$$

Defining $\theta \equiv (p/p^*)$, this becomes:

$$g^2(\theta) + 2\theta g(\theta) + 1 = 0$$

or (A-2)

$$g(\theta) = -\theta + \sqrt{\theta^2 + 1}$$

where the positive sign is chosen because $g(\theta)$ is an exponential, and therefore always positive.

The expression for ℓ then becomes:

$$\ell = \frac{4}{3} a^3 \left(\frac{2\pi}{mkt}\right)^{1/2} \left\{\frac{1}{1+\theta} + \frac{\pi}{4}\frac{\theta}{1+\theta} + \frac{3\pi}{128}\theta\left[1+\theta - \sqrt{\theta^2+1}\right]\right\} p^* \frac{d\theta}{dz} \tag{A-3}$$

Integrating from $\theta=0$ at $z=0$ to $\theta=\theta_s \equiv p_s/p^*$ at $z=L$ gives:

$$\ell = \frac{4}{3}\frac{a^3}{L}\, p^*\sqrt{\frac{2\pi}{mkt}}\left\{\frac{\pi}{4}\theta_s + \left(1-\frac{\pi}{4}\right)\ln\left(\theta_s+1\right) + \frac{\pi}{128}\left[\frac{3}{2}\theta_s^2 + \theta_s^3 - \left(\theta_s^2+1\right)^{3/2} + 1\right]\right\} \tag{A-4}$$

Using $\ell^* = \dfrac{\pi a^2 p_s}{(2\pi mkt)^{1/2}}$, (A-4) becomes

$$\ell = \left(\frac{8a}{3L}\right)\frac{\ell^*}{\theta_s}\left\{\frac{\pi}{4}\theta_s + \left(1-\frac{\pi}{4}\right)\ln\left(\theta_s+1\right) + \frac{\pi}{128}\left[\frac{3}{2}\theta_s^2 + \theta_s^3 - \left(\theta_s^2+1\right)^{3/2} + 1\right]\right\} \tag{A-5}$$

Setting $(8a/3L) \sim K$, (A-5) can be expressed in the form:

$$\ell = K\,\ell^*\,F(p_s/p^*) \tag{A-6}$$

If $F(p_s/p^*)$ is defined as:

$$F\left(\frac{p_s}{p^*}\right) = \frac{1}{(p_s/p^*)}\left\{\frac{\pi}{4}\left(\frac{p_s}{p^*}\right) + \left(1-\frac{\pi}{4}\right)\ln\left(\frac{p_s}{p^*}+1\right) + \frac{\pi}{128}\left[\frac{3}{2}\left(\frac{p_s}{p^*}\right)^2 + \left(\frac{p_s}{p^*}\right)^3 - \left(\left(\frac{p_s}{p^*}\right)^2+1\right)^{3/2} + 1\right]\right\} \tag{A-7}$$

(A-7) reduces to unity as $(p_s/p^*) \to 0$ and to $\frac{3\pi}{256}\left(\frac{p_s}{p^*}\right)$ as $(p_s/p^*) \to \infty$.

The fraction of total flow in each of the three regimes can be determined as a function of $(p_s/p^*) \equiv \theta_s$ as follows:

f_1 = fraction in viscous flow

f_2 = fraction in slip flow

f_3 = fraction in Knudsen flow

$$f_1 = \left(\frac{8}{3}\frac{a}{L}\right)\frac{1}{\theta_s}\left(\frac{\ell^*}{\ell}\right)\left(\frac{\pi}{128}\right)\left[\frac{3}{2}\theta_s^2 + \theta_s^3 - \left(\theta_s^2+1\right)^{3/2} + 1\right] \tag{A-8}$$

$$f_2 = \left(\frac{8}{3}\frac{a}{L}\right)\frac{1}{\theta_s}\left(\frac{\ell^*}{\ell}\right)\left(\frac{\pi}{4}\right)\left[\theta_s - \ln\left(\theta_s+1\right)\right] \qquad \text{(A-9)}$$

$$f_3 = \left(\frac{8}{3}\frac{a}{L}\right)\frac{1}{\theta_s}\left(\frac{\ell^*}{\ell}\right)\left[\ln\left(\theta_s+1\right)\right] \qquad \text{(A-10)}$$

These three quantities are shown in Figure 3.

APPENDIX B - Molecular Density Profile in a Short Tube

Consider a channel of length L and radius a. The pressure in the upstream reservoir is p_s, corresponding to a number density of $n_s = p_s/kT$. The pressure in the downstream reservoir into which the tube discharges is zero. The distance along the channel axis, z, is measured from the tube exit. The net flow per unit cross sectional area down the tube, $\ell/\pi a^2$, is independent of z and given by:

$$\ell/\pi a^2 = (1/4) n_s \bar{v} K \tag{B-1}$$

where K is the Clausing factor of Eq. (8). The speed distribution, $f_s(v)$, is assumed Maxwellian at all points in the tube, so that $\bar{v}$ is given by

$$\bar{v} = \int_0^\infty v f_s(v) dv = \left(\frac{8kT}{\pi m}\right)^{1/2}$$

Denote the angular distribution of the molecular flux by $f(\mu)$, where μ is the cosine of the angle between the velocity vector and the -z direction. The angular distribution is normalized so that:

$$\int_{-1}^{1} f(\mu) d\mu = 1$$

The average cosine of the angular distribution at any location is the first moment of the angular distribution:

$$\bar{\mu} = \int_{-1}^{1} \mu f(\mu) d\mu \tag{B-2}$$

At any point within the channel, the net current in the -z direction is the integral of the velocity component $v_{-z} = \mu v$ over all speeds and directions:

$$\ell/\pi a^2 = n(z) \int_0^\infty v f_s(v) dv \int_{-1}^{1} \mu f(\mu) d\mu = n(z) \bar{\mu}(z) \bar{v} \tag{B-3}$$

Since the net flow is independent of z, so is the product $n(z)\bar{\mu}(z)$.

Equating (B-1) and (B-3):

$$n(z)\,\bar{v}\bar{\mu}(z) = \frac{1}{4}\, n_s\, \bar{v}\, K \ ,$$

or

$$n(z) = \frac{n_s K}{4\bar{\mu}(z)} \tag{B-4}$$

If it is assumed that n(z) is linear, dn/dz will be constant, so that, differentiating Equation (B-3),

$$\bar{\mu}(z)\frac{dn}{dz} + n(z)\frac{d\bar{\mu}}{dz} = 0 \ ,$$

$$-\frac{d\bar{\mu}}{dz} = \frac{\bar{\mu}(z)}{n(z)}\,\frac{dn}{dz} \tag{B-5}$$

and

$$-\frac{1}{\left[\bar{\mu}(z)\right]^2}\,\frac{d\bar{\mu}}{dz} = \frac{1}{\bar{\mu}(z)n(z)}\,\frac{dn}{dz} = \text{constant} \tag{B-6}$$

Integrating this equation for $\bar{\mu}(z)$ with $\bar{\mu}(0) \equiv \mu_0$ and $\bar{\mu}(L) \equiv \bar{\mu}_L$ gives:

$$\frac{1}{\bar{\mu}(z)} = \frac{1}{\bar{\mu}_0} + \left[\frac{1}{\bar{\mu}_L} - \frac{1}{\bar{\mu}_0}\right]\left(\frac{z}{L}\right) \tag{B-7}$$

$\bar{\mu}_0$ is available from the measured angular distributions, since these represent the angular distribution of the current. In terms of the measured signals, $s(\mu)$, $\bar{\mu}_0$ is given by

$$\bar{\mu}_0 = \int_0^1 \left(s(\mu) - s_{bkg}\right) d\mu \Bigg/ \int_0^1 \left(s(\mu) - s_{bkg}\right)\frac{d\mu}{\mu}$$

$\bar{\mu}_0$ was found to be equal to 0.7 ± 0.02 for all sources at all pressures for which data was available.

$\bar{\mu}_L$ may be obtained from the approximate derivation of the short-tube Clausing factor.[16] In this derivation the orifice and tube are considered as series conductances, which is equivalent to assuming a pressure p_L to exist within the inlet end of the tube such that the total leak rate is given by:

$$\ell = \frac{a^2}{2}(p_s - p_L)\left(\frac{2\pi}{mkt}\right)^{1/2} = \frac{4}{3}\frac{a^3}{L}p_L\left(\frac{2\pi}{mkt}\right)^{1/2} \qquad \text{(B-8)}$$

where the first expression in (B-8) represents the leak rate through an orifice of radius a, and the second is the Knudsen expression for the leak rate through the tube, with negligible back pressure at the outlet. From (B-8)

$$p_s = p_L\left(1+\frac{8}{3}\frac{a}{L}\right) = \frac{8}{3}\frac{a}{L}p_L\left(1+\frac{3}{8}\frac{L}{a}\right) = \frac{8}{3}\frac{a}{L}\frac{p_L}{K} \qquad \text{(B-9)}$$

Since $p_L \propto n_L$, and $p_s \propto n_s$, (B-9) gives:

$$n_L = \left(\frac{3L}{8a}\right)Kn_s \qquad \text{(B-10)}$$

So that, from Equation B-4 evaluated at z=L:

$$n_L = \frac{n_s K}{4\mu_L} = \left(\frac{3L}{8a}\right)Kn_s \qquad \text{(B-11)}$$

$$\frac{1}{\bar{\mu}_L} = \frac{3}{2}\frac{L}{a} \qquad \text{(B-12)}$$

Combining Equation (B-7) and Equation (B-4),

$$n(z) = \frac{1}{4}n_s K\left[\frac{1}{\bar{\mu}_0} + \left(\frac{1}{\bar{\mu}_L} - \frac{1}{\bar{\mu}_0}\right)\frac{z}{L}\right] \qquad \text{(B-13)}$$

This can be rearranged to give:

$$n(z) = \frac{1}{4} n_s K \left(\frac{a}{L}\right) \left[\frac{1}{\bar{\mu}_L} - \frac{1}{\bar{\mu}_0}\right] \left\{ \frac{(L/a)}{\bar{\mu}_0} \left(\frac{1}{\bar{\mu}_L} - \frac{1}{\bar{\mu}_0}\right)^{-1} + \frac{z}{a} \right\} \quad \text{(B-14)}$$

or, in summary,

$$n(z) = \frac{n_s}{\beta} \left(\alpha + \frac{z}{a}\right) \quad \text{(B-15)}$$

$$\beta = \frac{4L}{aK} \left(\frac{1}{\bar{\mu}_L} - \frac{1}{\bar{\mu}_0}\right)^{-1} \; ; \; \alpha = \frac{\beta K}{4\bar{\mu}_0} \quad \text{(B-16)}$$

$$\bar{\mu}_0 = 0.7 \; ; \; \bar{\mu}_L = \frac{2}{3} \frac{a}{L}$$

APPENDIX C - Theoretical Peaking Factor Calculation

The peaking factor χ is calculated as a function of reduced driving pressure for a single tube of circular cross section. The tube radius is a, the length is L, and z is the distance measured from the low pressure end of the tube. We assume that the mean free path λ at the source pressure p_s is larger than the tube radius a. A linear variation of gas density with z is assumed:

$$n(z) = \frac{n_s}{\beta}\left(\alpha + \frac{z}{a}\right) \qquad \text{(C-1)}$$

where the constants α,β are derived in Appendix B.

Following Giordmaine and Wang (8), the centerline intensity, J(0), is the sum of two contributions.

$J_1(0)$ = Molecules heading forward after intermolecular collisions which occur inside the channel.

$J_2(0)$ = Molecules from the source which pass through the channel uncollided.

Consider an element of volume $\pi a^2 dz$ at distance z from the exit of the channel. The number of collisions within this volume element is $(n(z)\ \bar{v})\ (\sqrt{2}\ n(z)\pi\sigma^2)\ (\pi a^2 dx)$ where $\bar{v}$ is the mean velocity and σ is the collision diameter. Assuming isotropic scattering in the laboratory system, these collisions result in

$$\sqrt{2}\ \pi^2\ \sigma^2\ a^2\ \bar{v}\ [n(z)]^2\ dz\ \frac{d\omega}{4\pi}$$

molecules.

traveling into solid angle $d\omega$. Of these molecules heading toward the exit, a fraction $e^{-z/\bar{\lambda}(z)}$ will escape, where $\bar{\lambda}(z)$ is the average mean free path over the remaining length of channel. The contribution to forward intensity from collisions in $\pi a^2 dz$ is

$$d[J_1(0)]\, d\omega = \frac{\pi\sigma^2}{2\sqrt{2}}\, a^2 \bar{v}\, [n(z)]^2\, e^{-z/\bar{\lambda}(z)} dz d\omega \qquad \text{(C-2)}$$

The average mean free path is computed by:

$$\bar{\lambda}(z) = z \Big/ \int_0^z \frac{dz'}{\lambda(z')} \qquad \text{(C-3)}$$

$$\lambda(z') = \frac{1}{\sqrt{2}\, \pi\sigma^2 n(z)}$$

Using (C-1), $\bar{\lambda}(z)$ becomes

$$\frac{1}{\bar{\lambda}(z)} = \sqrt{2}\, \pi\, \sigma^2\, \frac{n_s}{\beta} \left(\alpha + \frac{1}{2}\frac{z}{a}\right) \qquad \text{(C-4)}$$

The total collision contribution $J_1(0)$ is computed by integrating (C-2) from z = 0 to L. Utilizing the above expressions for $\bar{\lambda}(z)$, n(z) and making the substitutions $u = z/a$, $\ell^* = 1/4 n_s \bar{v}\, \pi a^2$, and $p_s/p^* = 2a(\sqrt{2}\pi\sigma^2 n_s)$, we obtain:

$$J_1(0) = \frac{\ell^*}{2\pi\beta^2} \left(\frac{p_s}{p^*}\right) \int_0^{L/a} (\alpha + u)^2 \exp\left\{ - \left(\frac{p_s}{p^*}\right)\left(\frac{\alpha u + u^2/2}{2\beta}\right) \right\} du \qquad \text{(C-5)}$$

With a change of variable to $w = u + \alpha$, and using $\nu^2 = \frac{p_s/p^*}{4\beta}$ the integral simplifies to a form $\int w^2 \, e^{-\nu^2 w^2} dw$ which is then integrated by parts to yield $J_1(0)$.

$$J_1(0) = \frac{\ell^*}{\pi\beta} \, e^{\nu^2 d^2} \left\{ \nu\alpha \, e^{-\nu^2\alpha^2} - \nu(\alpha + \frac{L}{a}) \, e^{-\nu^2 (\alpha + \frac{L}{a})^2} + \right.$$

$$\left. \frac{\sqrt{\pi}}{2} \left[\operatorname{erf}\left(\nu \, (\alpha + \frac{L}{a})\right) - \operatorname{erf} (\nu\alpha) \right] \right\} \qquad \text{(C-6)}$$

The uncollided centerline intensity $J_2(0)$ is given by,

$$J_2(0) = \frac{1}{4} a^2 n_s \bar{v} \, e^{-L/\bar{\lambda}} \, (L) \qquad \text{(C-7)}$$

The total centerline intensity, $J(0)$ is the sum of (C-6) and (C-7).

The peaking factor is defined as the ratio of the centerline intensity from the channel source to that from an ideal thin-walled orifice when both are emitting the same number of molecules per second.

The leak rate from a capillary of Clausing factor $K = 1/(1+3L/8a)$, radius a, and source pressure p_s (corresponding to gas density n_s) is $\ell = K\ell^*$. The centerline intensity of a thin-walled orifice emitting $K\ell^*$ molecules/sec is $\frac{K\ell^*}{\pi}$, so the peaking factor becomes,

$$\chi = \frac{J(0)}{K\ell^*/\pi} = \frac{J_1(0) + J_2(0)}{K\ell^*/\pi} \qquad \text{(C-8)}$$

Substituting (C-6) and (C-7) into (C-8) yields

$$\chi = \frac{1}{K} e^{-L/\bar{\lambda}(L)} + \frac{1}{K\beta} e^{\alpha^2\nu^2} \left\{ \nu\alpha\, e^{-\nu^2\alpha^2} - \nu(\alpha + \frac{L}{a})\, e^{-\nu^2(\alpha + \frac{L}{a})^2} + \right.$$

$$\left. \frac{\sqrt{\pi}}{2} \left[\operatorname{erf}\left(\nu(\alpha + \frac{L}{a})\right) - \operatorname{erf}(\nu\alpha) \right] \right\} \qquad \text{(C-9)}$$

After substituting for $\bar{\lambda}(L)$ and ν and rearranging terms, Eq.(19) results.

APPENDIX D - Effect of Probe Length on Detection Efficiency

The rate at which first flight molecules from the source enter the front face of the probe is $J(0)\pi a_p^2/d^2$. If the solid angle is computed to the back of the probe tube instead of the front, only a fraction $[d/(d+L_p)]^2$ of the molecules entering the front face are transmitted without wall collision. Some of the remainder which strike the walls will be rejected back to the vacuum chamber. For a non-directed gas (such as the background gas) entering the front face of the probe, only a fraction K_p reach the back face, where K_p is the Clausing factor of the probe. However, since the first flight flux to the probe face is much more collimated than a non-directed gas, it will be assumed that the fraction of those molecules on the outer periphery of the entrance solid angle which strike the walls but succeed in reaching the back face is $2K_p$. Thus, of the total number of first flight molecules which enter the front face of the probe, the fraction which reach the back face and are fed to the leak detector is

$$\left(\frac{d}{d+L_p}\right)^2 + 2K_p\left(\frac{L_p}{d+L_p}\right)^2 = \left(\frac{5}{5+0.63}\right)^2 + (2)\ (0.072)\left(\frac{0.63}{5+0.63}\right)^2 = 0.81$$

APPENDIX E - Signal-to-Background Ratio of Detector Probe

The ratio of the first flight signal along the centerline to the background signal is defined as the "signal-to-background ratio"

$$\rho = \frac{s(0) - s_{bkg}}{s_{bkg}} \qquad \text{(E-1)}$$

This ratio can be computed for a particular experimental design in the following manner. The first flight flow down the probe when $\theta = 0$ is denoted by $\nu_{ff}(0)$ molecules/sec. If the radius of the probe tube is a_p and the distance between the source tip and the probe is d, the solid angle subtended by the probe opening as seen from the source tip is $\pi a_p^2/d^2$. The total rate at which molecules enter the probe tube is the centerline intensity from the source, $J(0)$, times this solid angle. If the source and probe are properly aligned on the source axis, most of the entering molecules travel down the length of the probe tube without colliding with the walls, since they enter the probe well collimated. However, even with perfect alignment, the portion of the molecules which enter the probe near the periphery of the solid angle of the opening will strike the walls of the tube and may be returned to the vacuum chamber. Determination of the fraction of the molecules entering the front face of the probe which reach the opening is shown in Appendix D to be approximately 0.81 for the design used here. Expressing $J(0)$ in terms of the total source leak rate and peaking factor by Eq. (13), the flow down the probe tube due to first flight from the source is

$$\nu_{ff}(0) = 0.81\chi\ell(a_p/d)^2 \qquad \text{(E-2)}$$

The rate at which background gas flows down the probe tube is given by the orifice formula, Eq. 2, multiplied by the Clausing factor of the probe

$$\nu_{bkg} = K_p \frac{3.51\times10^{22}}{\sqrt{MT}} p_o (\pi a_p^2) \qquad \text{(E-3)}$$

With the pressure of helium in the vacuum chamber given by $\ell/3.24\times10^{19}S_o$, we obtain

$$\nu_{bkg} = \frac{3.51\times10^{22}}{3.24\times10^{19}} \frac{K_p}{\sqrt{MT}} \frac{\pi a_p^2}{S_o} \ell \qquad \text{(E-4)}$$

The numerator of Eq. (E-1) is proportional to $\nu_{ff}(0)$, while the denominator is proportional to ν_{bkg}. The signal-to-background ratio becomes

$$\rho = \chi\rho^* \qquad \text{(E-5)}$$

where, for M = 4 (helium) and T = 300°K,

$$\rho^* = \frac{8.25\times10^{-3} S_o}{K_p d^2} \qquad \text{(E-6)}$$

ρ^* is the centerline signal-to-background ratio which would be observed if the source were an ideal orifice. ρ^* increases with pumping speed, since a larger pump can maintain a lower helium background pressure. Small probe Clausing factors increase ρ^* by impeding the flow of background

gas down the probe without significantly reducing the first flight contribution. The inverse variation of ρ^* with d^2 due to the solid angle subtended by the probe opening strongly suggests that the distance d be as small as possible consistent with adequate angular resolution of the probe. The parameters ρ and χ are directly measured in the experiment. According to Eqs. (E-5) and (E-6), the ratio ρ/χ should be constant for all sources and all source pressures. For the apparatus used here, S_o = 500 lit/sec (nominal), K_p = 0.072, and d = 5 cm, from which

$$\rho^* = 2.3$$

NOTATION

a = radius of source aperture, cm.

a_p = radius of probe aperture, cm.

A = cross sectional area of source aperture, cm^2.

B = constant (for a given gas), Eq. (4).

C_s = source conductance, lit/sec.

d = distance between emitting source and collimator or probe, cm.

$F(p_s/p^*)$ = leak rate correction factor due to Fryer, Eq. (12).

$J(0)$ = angular emission pattern, molecules/sr-sec.

$J^*(0)$ = angular emission pattern from an ideal orifice.

$J_1(0)$ = centerline emission intensity due to collided molecules.

$J_2(0)$ = centerline emission intensity due to uncollided molecules.

k = Boltzmann constant.

K = Clausing factor, Eq. (8).

K_p = Clausing factor of probe.

ℓ = total leak rate, molecules/sec.

ℓ^* = leak rate from an ideal thin-walled orifice, molecules/sec.

L = length of source channel, cm.

L_p = length of probe channel, cm.

m = molecular mass, gm/molecule.

M = molecular weight, gm/mole.

N = number of channels in multichannel source.

$n(z)$ = gas density at position z in source channel, molecules/cm^3.

p_s = pressure in source tube reservoir.

p_o = pressure in source chamber.

p^* = source pressure at which the mean free path is equal to the channel diameter, Eq. (9).

r_1 = radius of collimating orifice, cm.

R = gas constant.

$s(\theta)$ = measured signal at angle θ.

S_o = pump speed, lit/sec.

T = absolute temperature, °K.

$\bar{v}$ = mean thermal velocity of gas, cm/sec.

V_r = volume of reservoir, lit.

z = distance along axis of source channel, measured from low pressure end, cm.

GREEK SYMBOLS

θ = polar angle of emission pattern.

σ = kinetic theory collision diameter of gas molecule.

ρ = signal-to-background ratio.

ρ^* = signal-to-background ratio if source is an ideal orifice.

ν = flow down probe, molecules/sec.

η = parameter, Eq. (27).

μ = viscosity.

$\bar{\mu}$ = average cosine of molecular flux.

λ = mean free path of effusing gas.

τ = transmissivity of source, Eq. (26).

χ = peaking factor, Eq. (13).

References

1. S. Datz, G. E. Moore, and E. H. Taylor, Advances in Rarefied Gas Dynamics, J. A. Laurmann, Ed., Vol. 1, Suppl. 2, (Academic Press, New York, 1963) p. 347.
2. J. N. Smith and W. L. Fite, Advances in Rarefied Gas Dynamics, J. A. Laurmann, Ed., Vol. 1, Suppl. 2, (Academic Press, New York, 1963) p. 430.
3. R. A. Krakowski, (Ph.D. Thesis), University of California, Berkeley, UCRL-17336, (1967).
4. W. Steele, AFML-TR-65-343 (1965).
5. H. Pauly and J. P. Toennies, Adv. in Atomic and Molecular Phys., 1, 201 (1965).
6. J. B. Anderson, R. P. Andres, and J. B. Fenn, Adv. in Atomic and Molecular Phys., 1, 345 (1965).
7. G. M. Fryer, Trans. Faraday Soc., 293A, 329 (1966).
8. J. A. Giordmaine and T. C. Wang, J. Appl. Phys., 31, 463 (1960).
9. M. Sibulkin and W. H. Gallaher, A.I.A.A. J., 1, 1452 (1963).
10. G. R. Hanes, J. Appl. Phys., 31, 2171 (1960).
11. J. C. Johnson, A. T. Stair, Jr., and J. L. Pritchard, J. Appl. Phys., 37, 1551 (1966).
12. P. B. Scott, AFOSR 65-0192 (1965).
13. F. A. Scott and F. A. L. Dullien, A.I.Ch.E. J., 8, 293 (1962).
14. R. E. Stickney, R. P. Keating, S. Yamumoto and W. J. Hastings, J. Vac. Sci. and Tech. 4, 10 (1967).
15. W. L. Winterbottom, J. Chem. Phys. 47, 3546 (1967).
16. M. Pirani and J. Yarwood, "Principles of Vacuum Engineering", p. 11, Reinhold (New York) (1961).

FIGURE CAPTIONS

1. Typical apparatus for a molecular beam experiment.
2. Fryer's capillary flow equation for zero downstream pressure (Eq. (12)).
3. Fraction of total flow in each regime, after Fryer.
4. Peaking factor measurements of Giordmaine and Wang - source A.
5. End view of apparatus.
6. Side view of apparatus.
7. Schematic of Apparatus.
8. Helium pressure decay curve for single capillary source.
9. Angular distribution from single capillary source with source pressure of 1.06 torr.
10. Peaking factors as a function of reduced source pressure for single capillary source.
11. Krinkly foil source (after ref. 3).
12. Angular distribution from Krinkly foil source at 1.0 torr - slot horizontal.
13. Angular distribution from Krinkly foil source at 1.0 torr - slot vertical.
14. Peaking factors of Krinkly foil source as a function of reduced source pressure.
15. Quartz membrane source (50 x).
16. Pressure decay curve of quartz membrane source for helium.
17. Peaking factors as a function of reduced source pressure for quartz membrane source.
18. Mosaic Source A (100X). the lighter region contains the open channels.
19. Mosaic Source B (50X). the dark spots are the open channels.

20. Pressure decay curve of Mosaic source A for helium.

21. Pressure decay curve of Mosaic source B for helium.

22. Angular distribution from Mosaic source A at 1.0 torr.

23. Peaking factor as a function of reduced source pressure for Mosaic source A.

24. Peaking factor as a function of reduced source pressure for Mosaic source B.

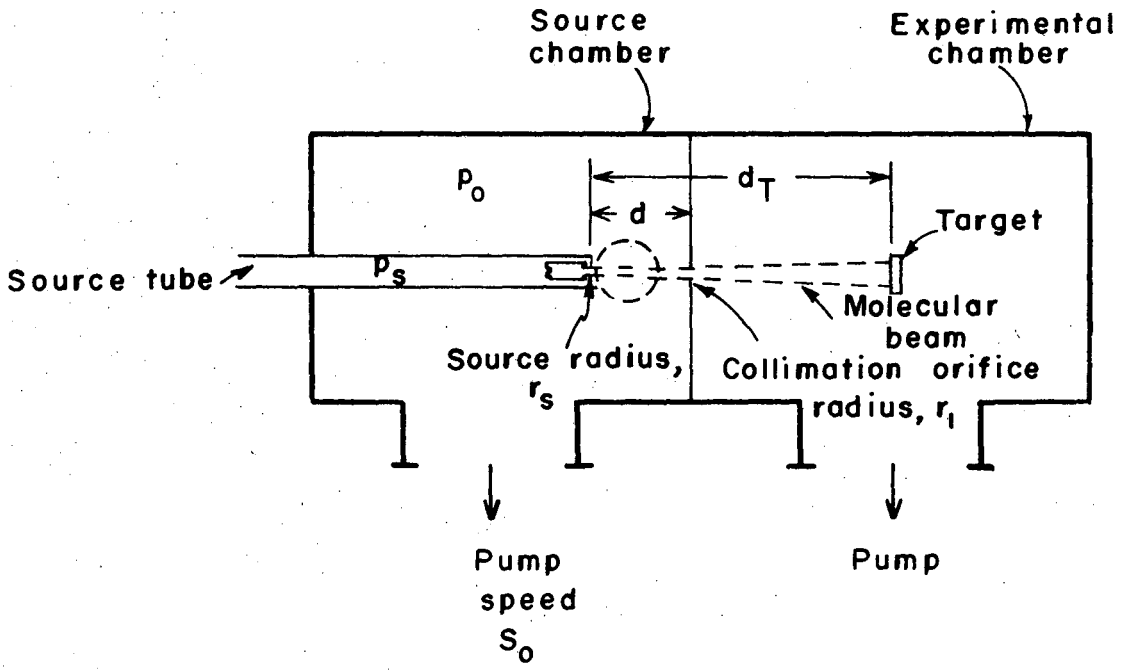
Source chamber
Experimental chamber
p_o
d_T
d
Target
Source tube
p_s
Molecular beam
Source radius, r_s
Collimation orifice radius, r_1
Pump speed S_o
Pump
XBL6811-7170

Fig. 1

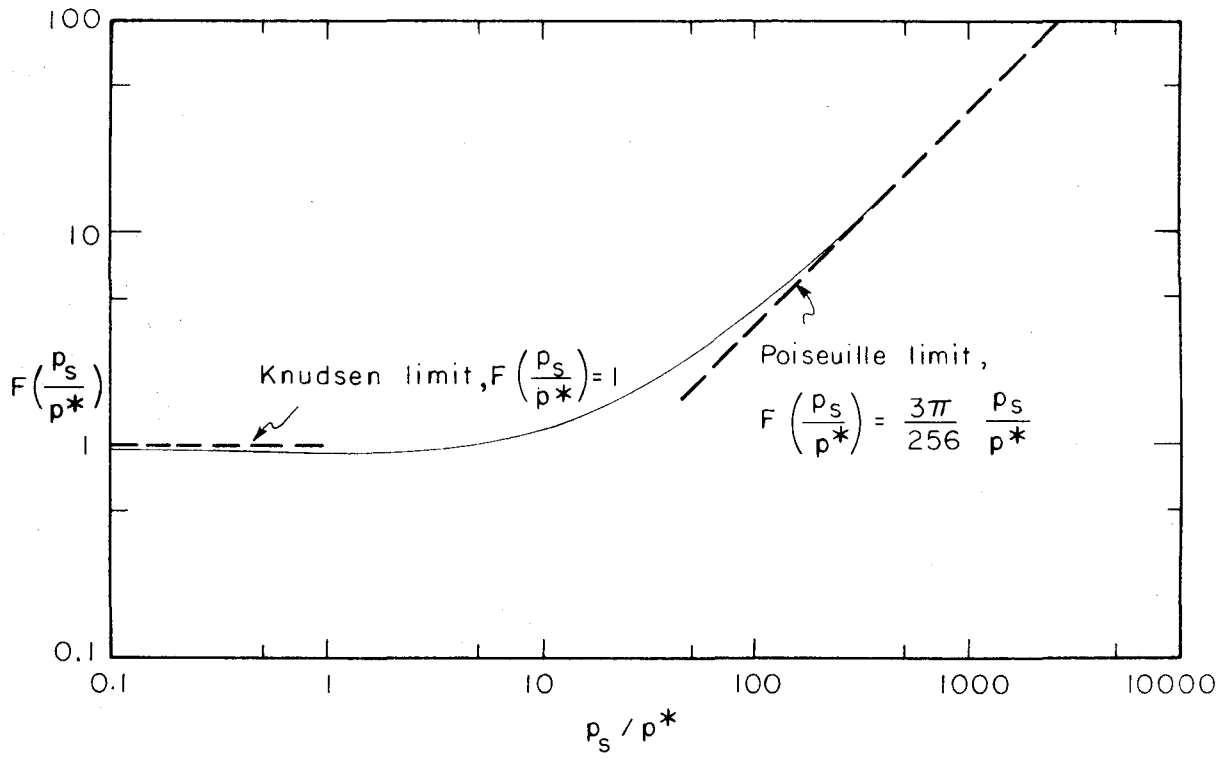
100
10
1
0.1
0.1
1
10
100
1000
10000
$F\left(\frac{p_s}{p^*}\right)$
p_s / p^*
Knudsen limit, $F\left(\frac{p_s}{p^*}\right)=1$
Poiseuille limit,
$F\left(\frac{p_s}{p^*}\right) = \frac{3\pi}{256}\frac{p_s}{p^*}$
XBL6811-7171

Fig. 2

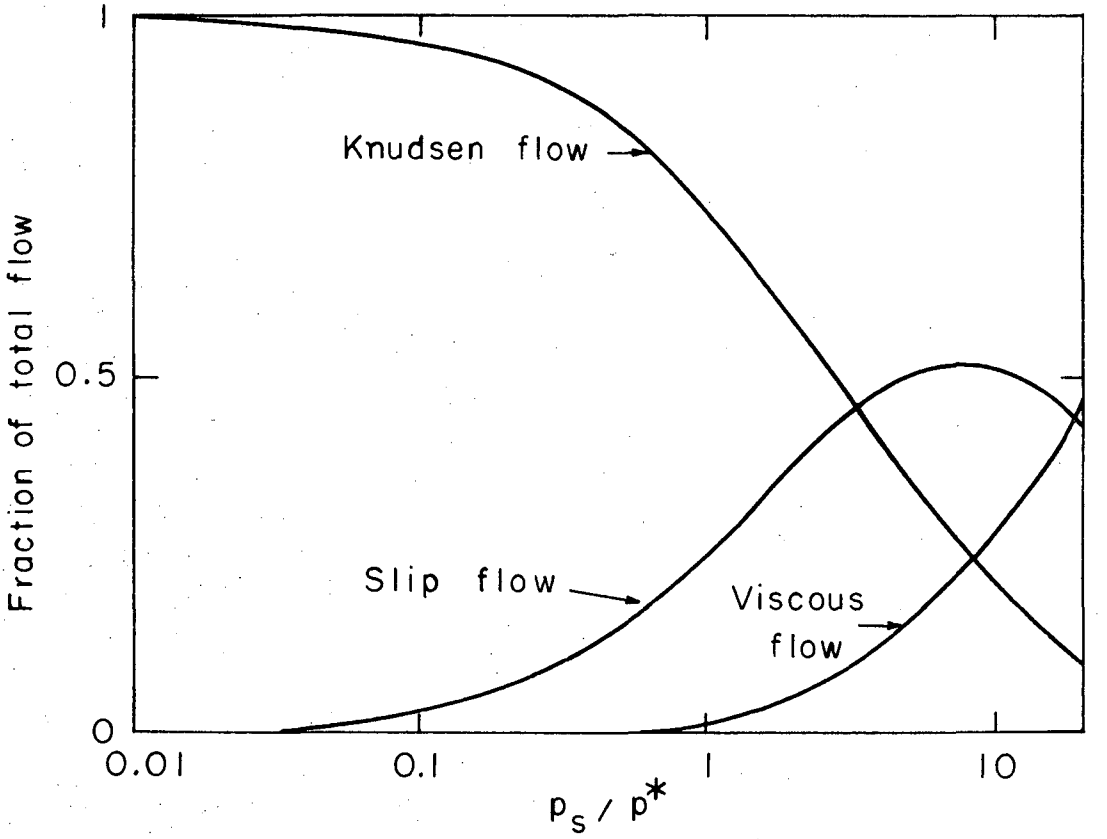

XBL6811-7172

Fig. 3

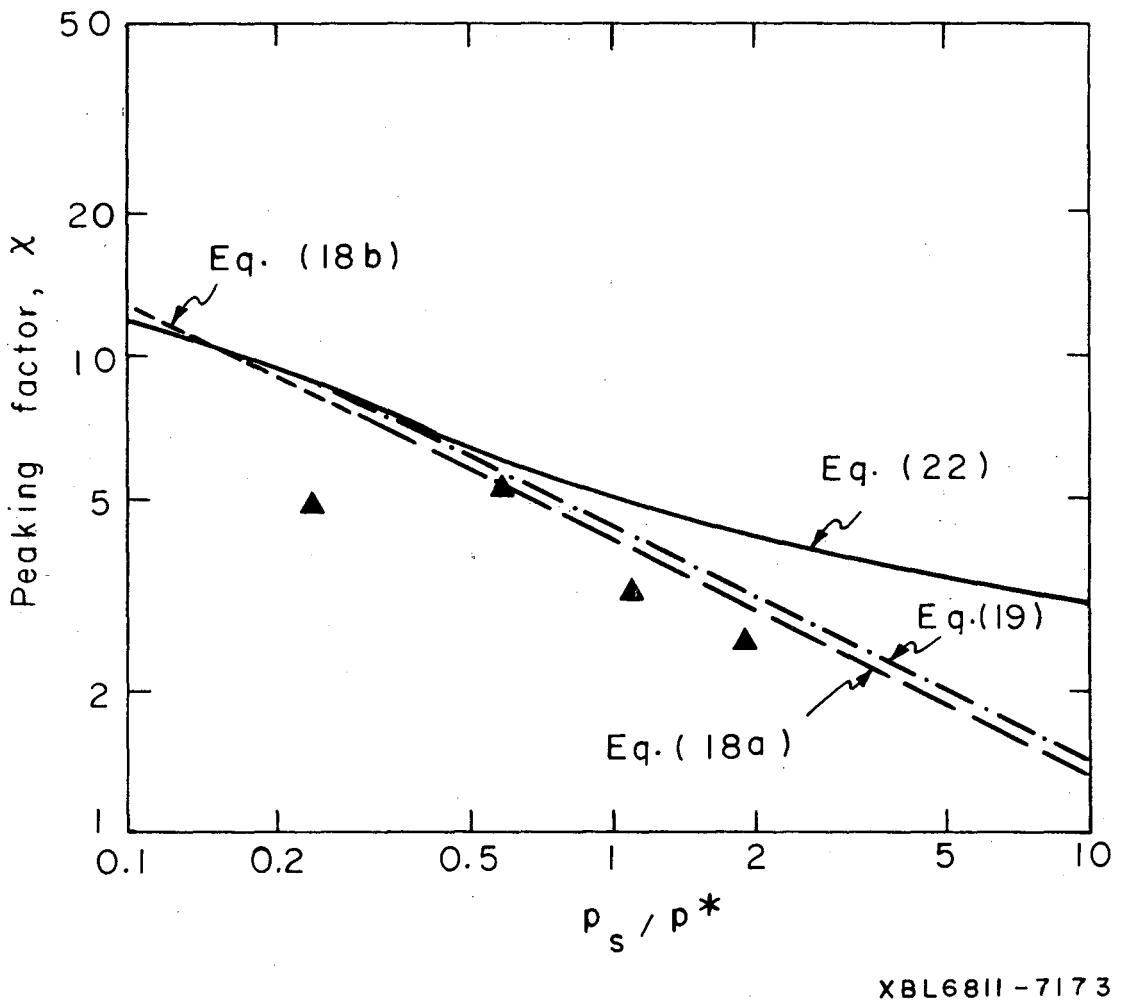
50
20
10
5
2
1
0.1
0.2
0.5
1
2
5
10
Peaking factor, χ
p_s / p^*
Eq. (18b)
Eq. (22)
Eq.(19)
Eq. (18a)
XBL6811-7173

Fig. 4

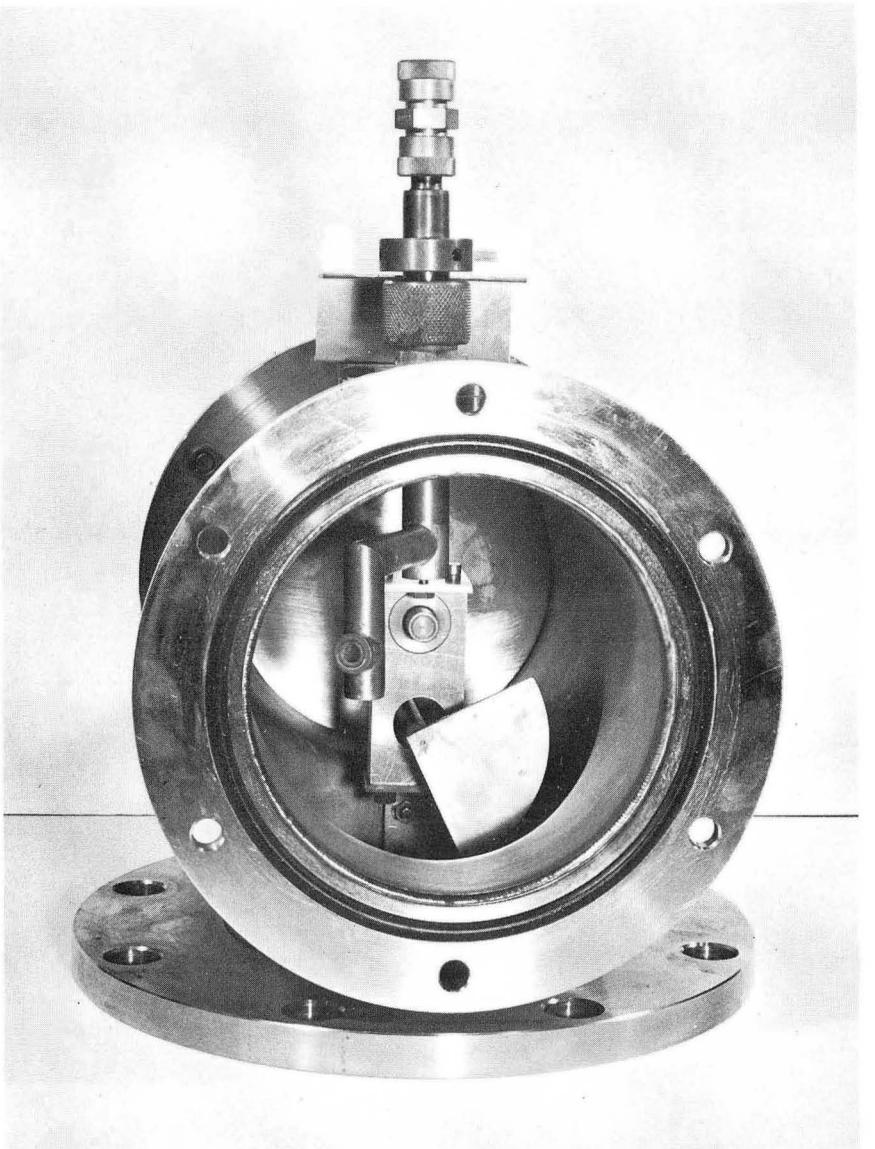

XBB 6811-6910

Fig. 5

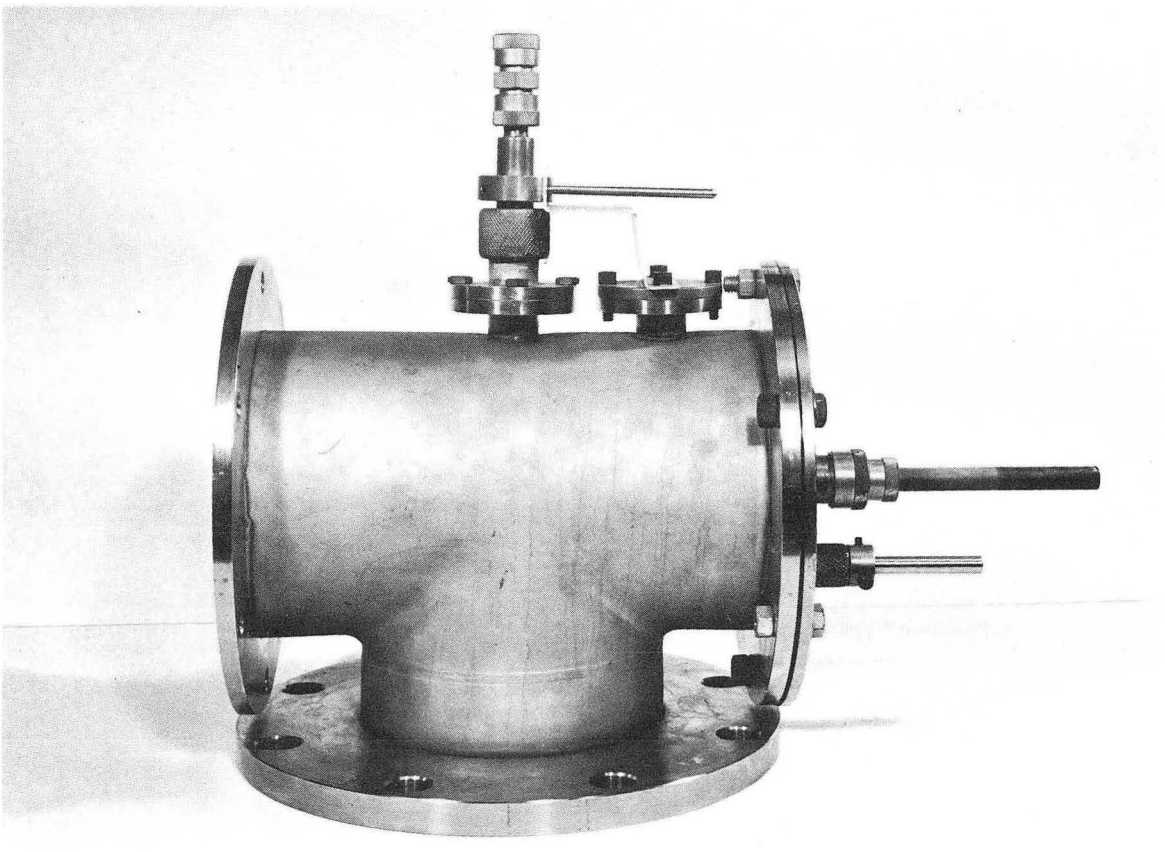

XBB 6811-6911

Fig. 6

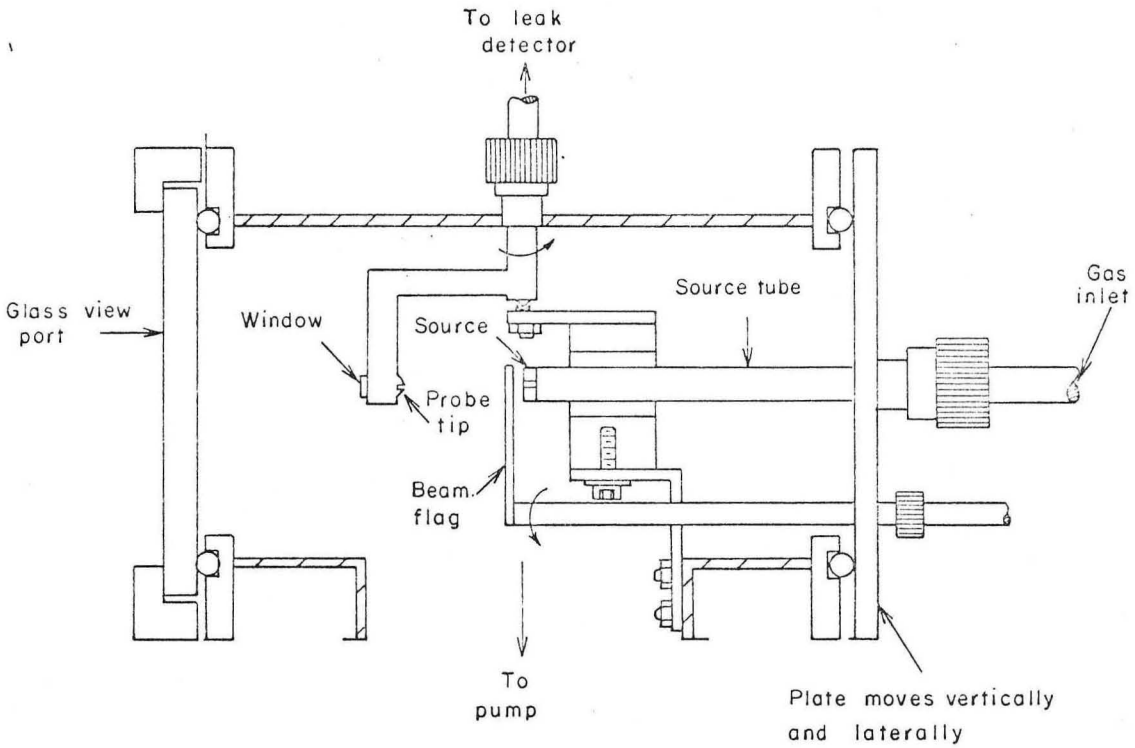

XBL6811-7174

Fig. 7

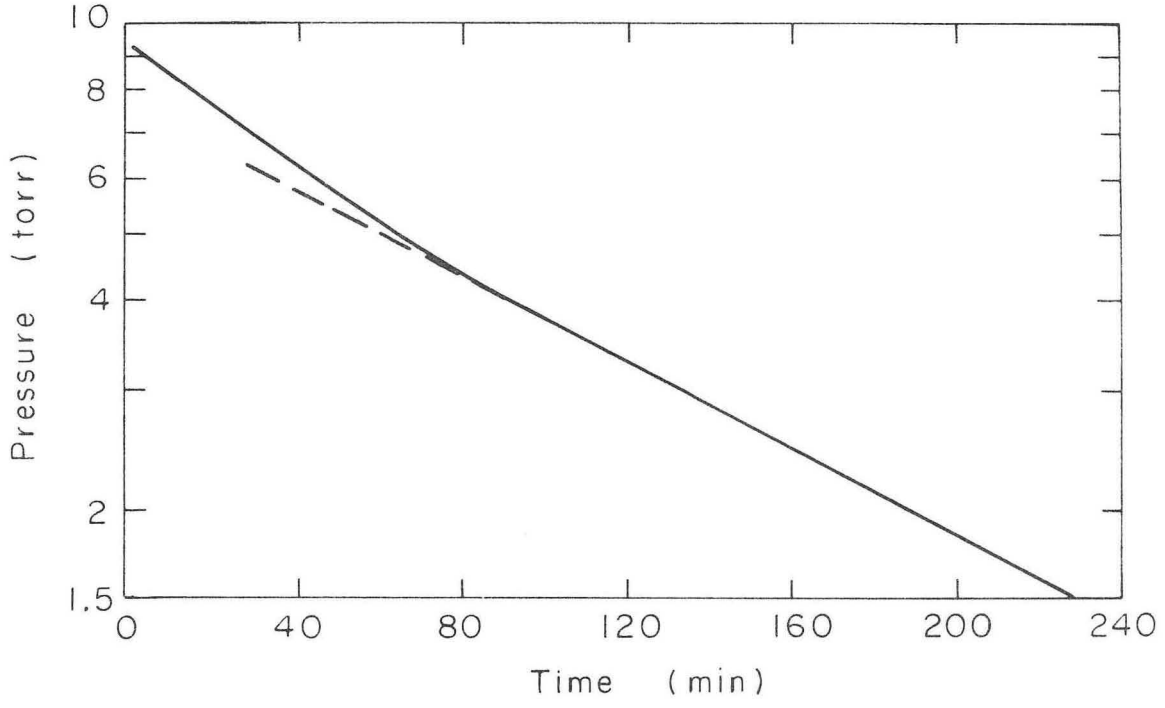

XBL 6811-7151

Fig. 8

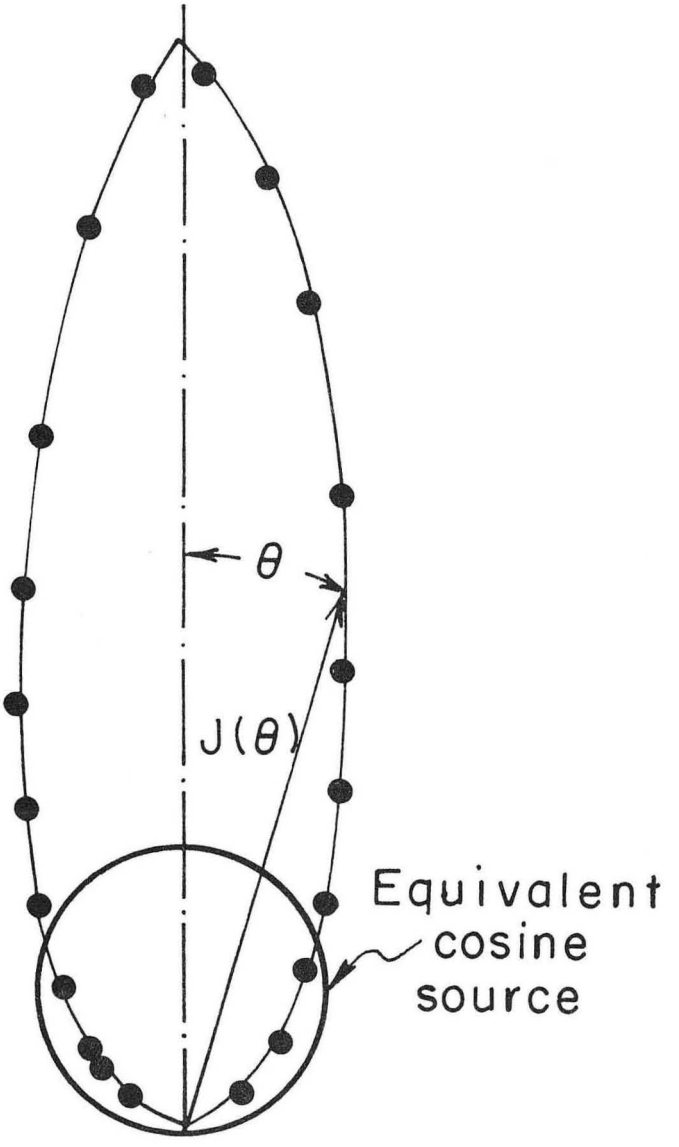

XBL 6811-7176

Fig. 9

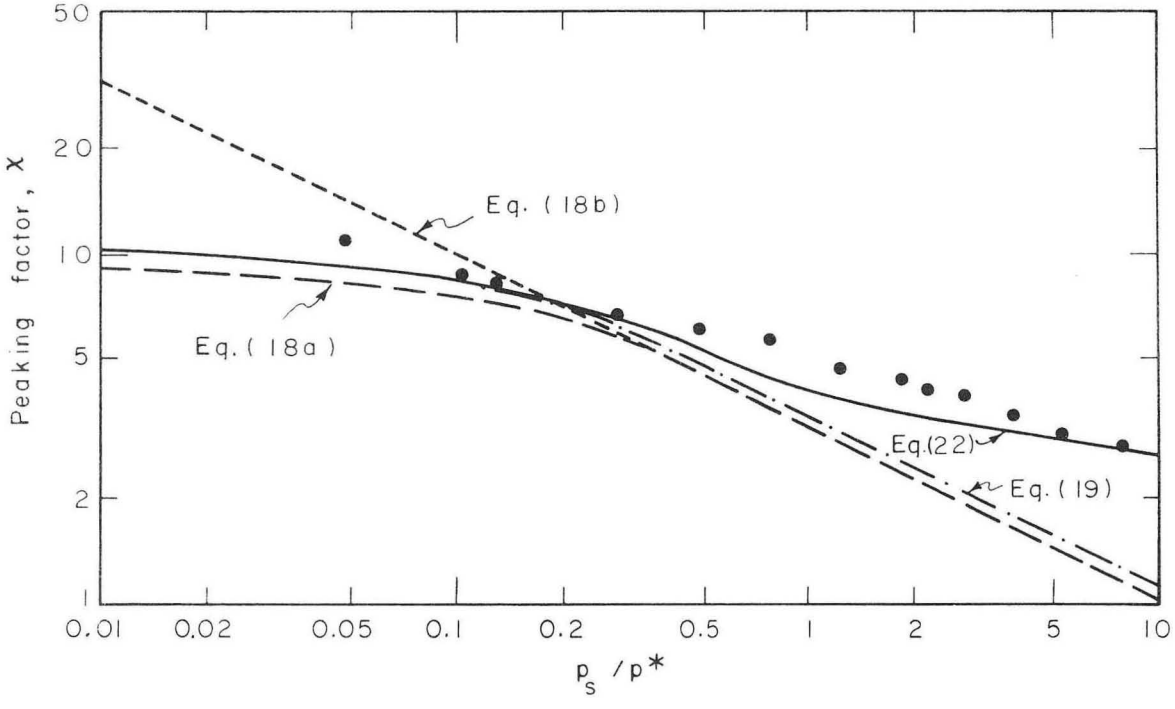
50
20
10
5
2
1
Peaking factor, χ
Eq. (18b)
Eq. (18a)
Eq.(22)
Eq. (19)
0.01
0.02
0.05
0.1
0.2
0.5
1
2
5
10
p_s / p^*
XBL6811-7177

Fig. 10

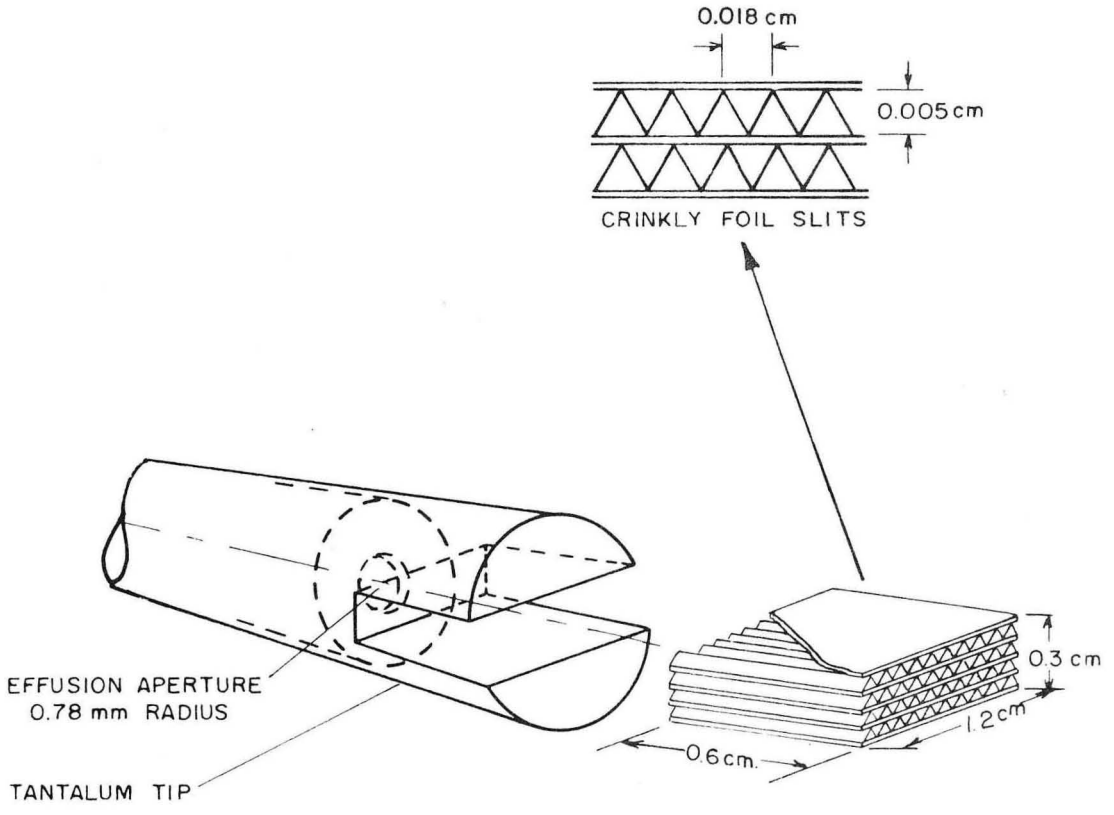

XBL 672-554-A

Fig. 11

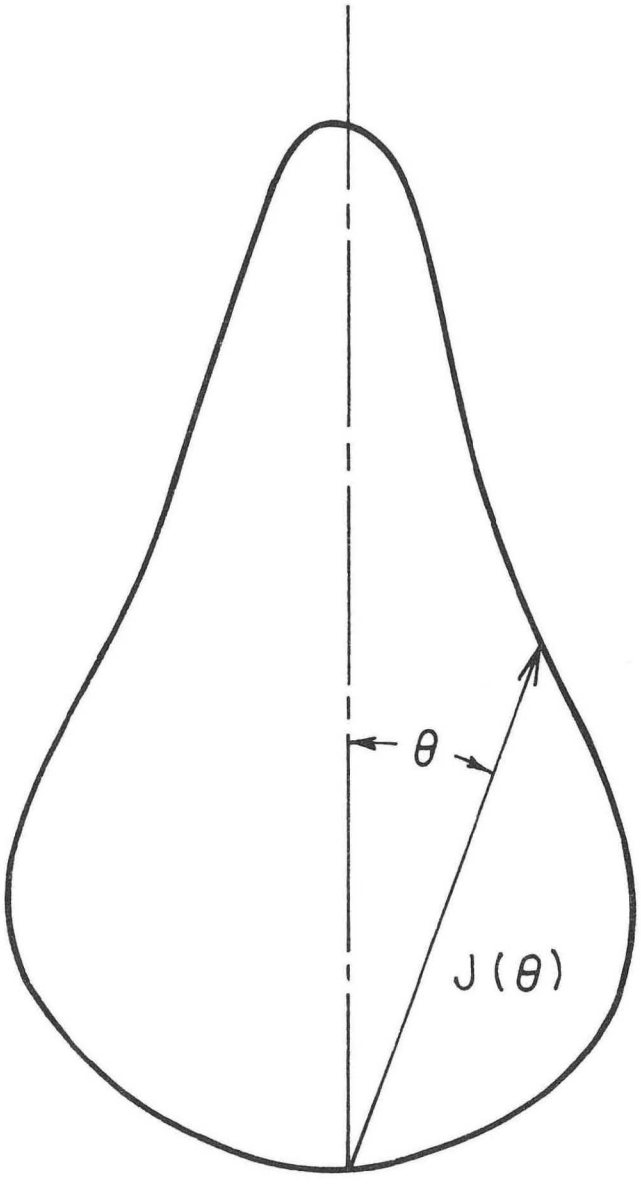

XBL6811-7178

Fig. 12

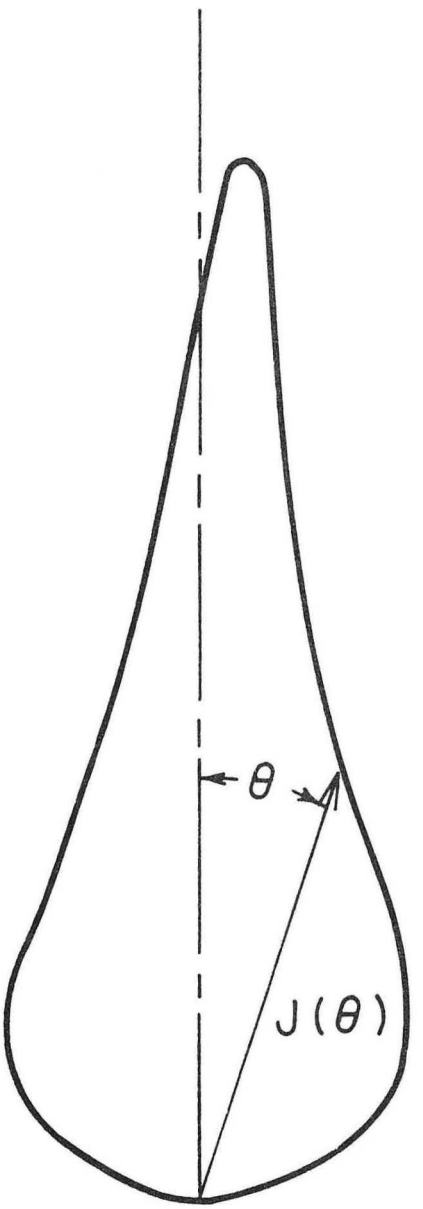

XBL6811-7179

Fig. 13

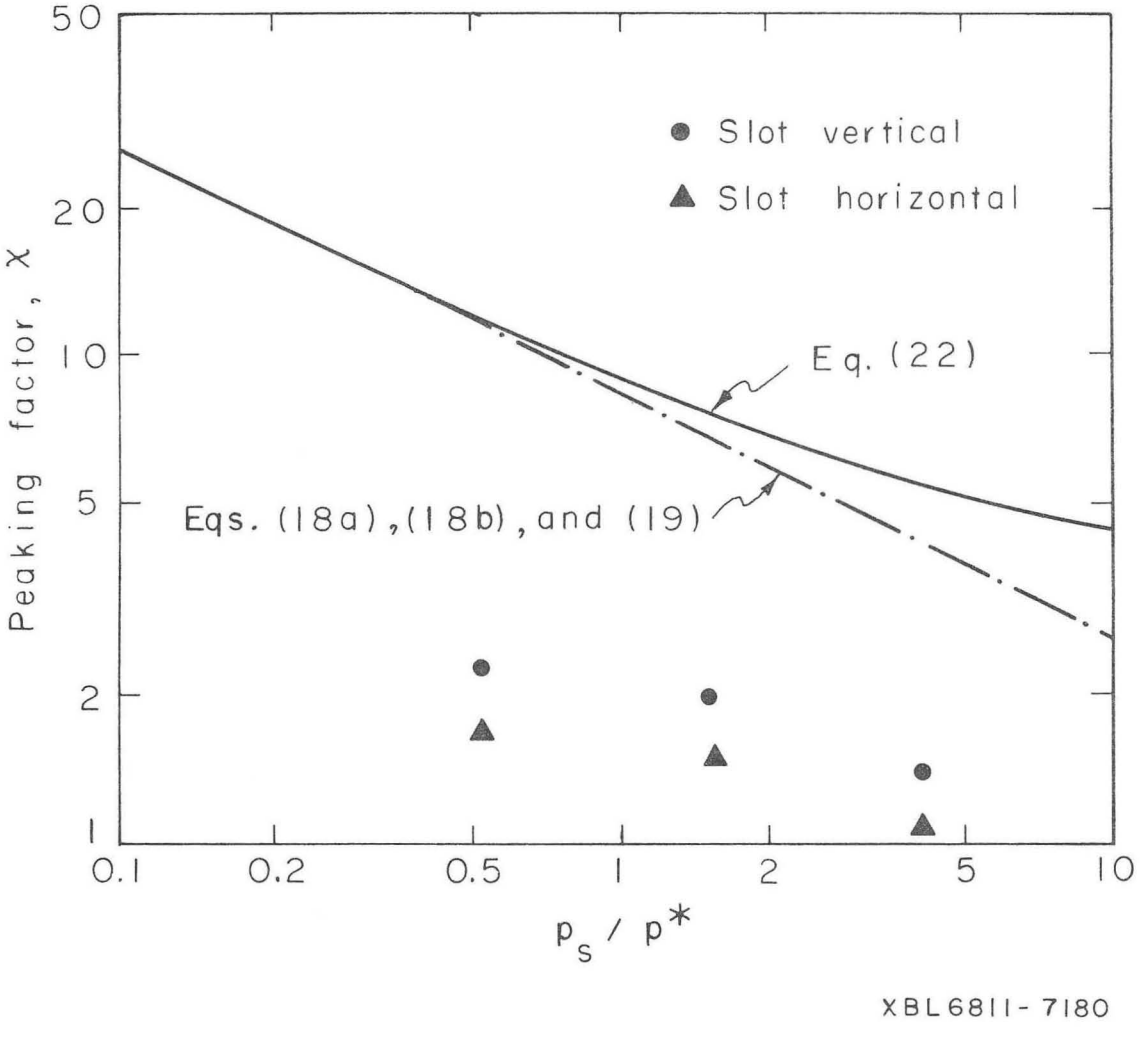
50
20
10
5
2
1
0.1
0.2
0.5
1
2
5
10
Peaking factor, χ
p_s / p^*
Slot vertical
Slot horizontal
Eq. (22)
Eqs. (18a), (18b), and (19)
XBL6811-7180

Fig. 14

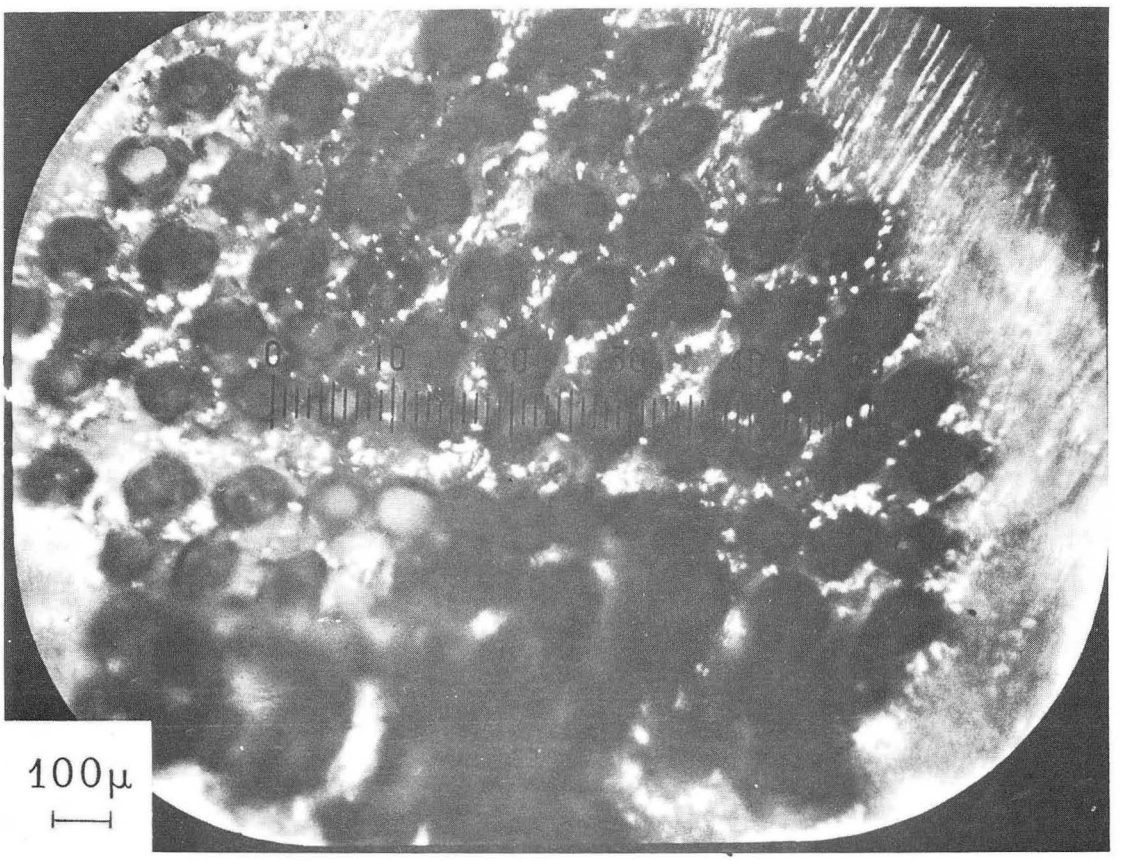

XBB 6811-7098

Fig. 15

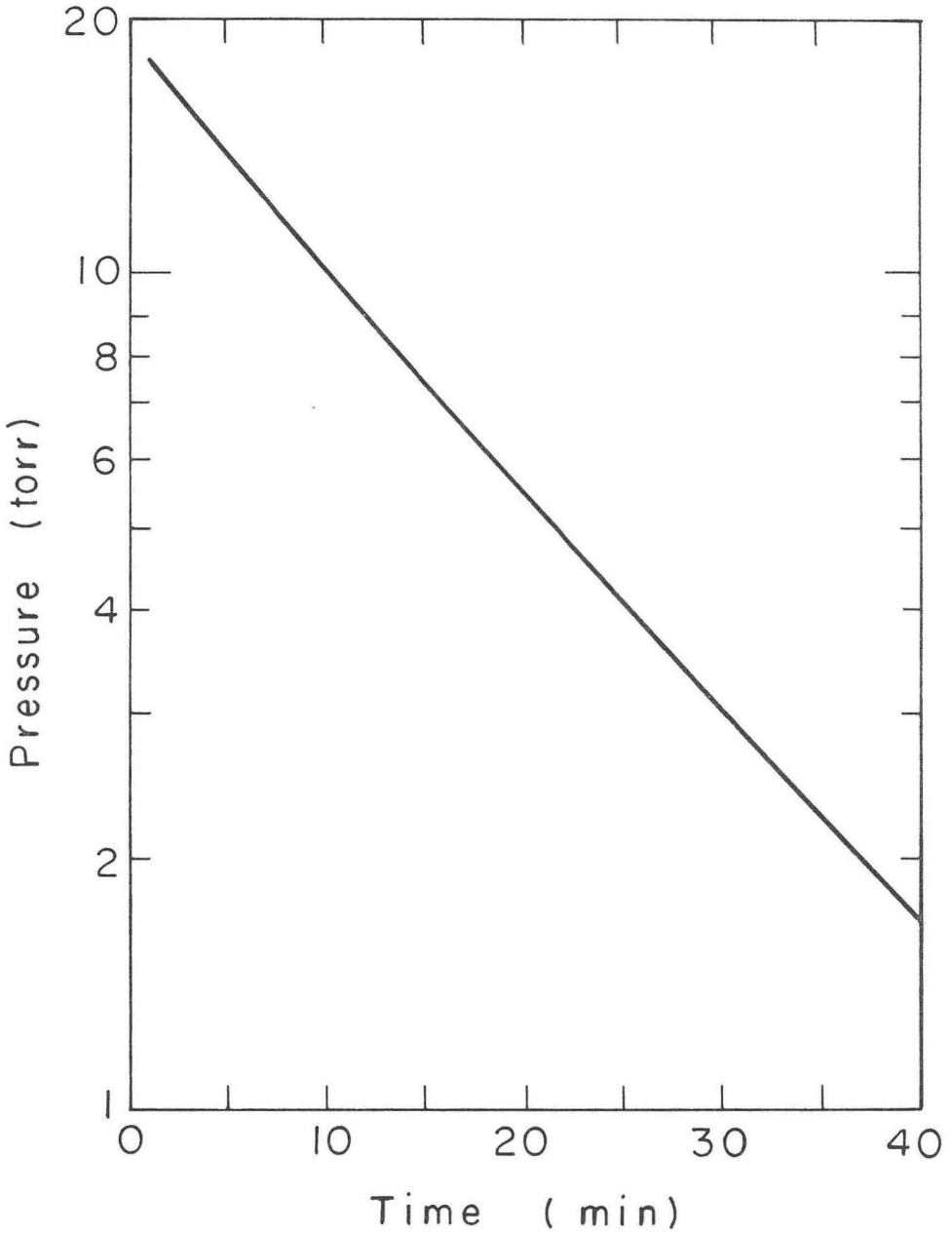

Fig. 16

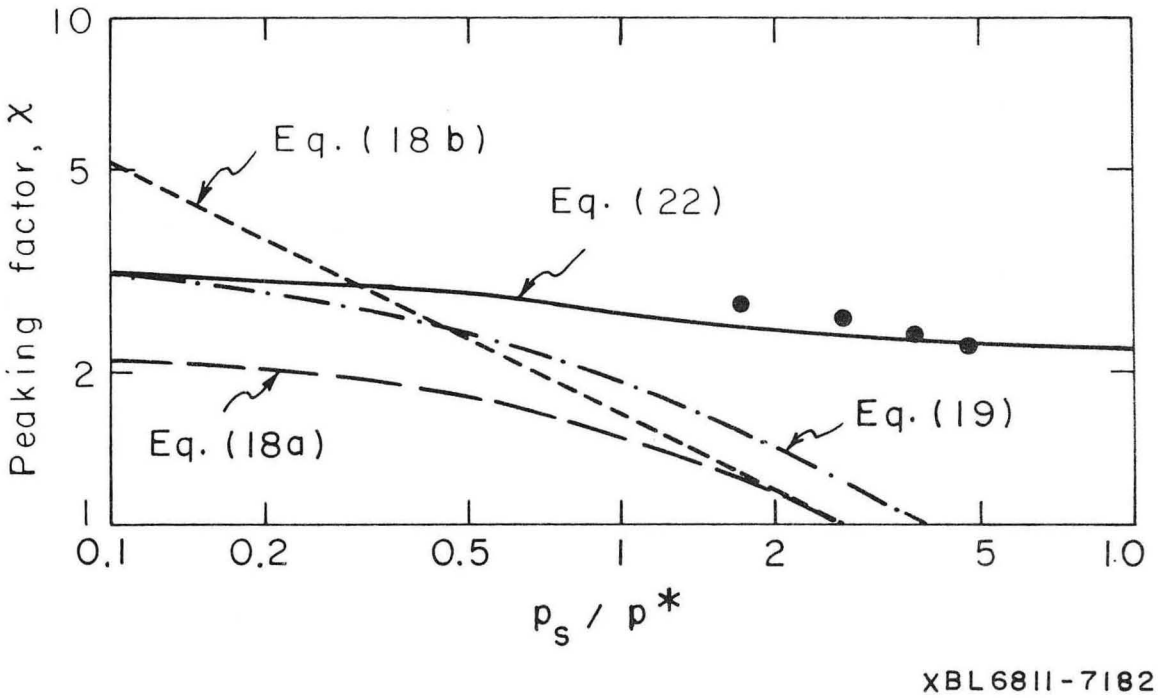
10
5
2
1
Peaking factor, χ
Eq. (18b)
Eq. (22)
Eq. (19)
Eq. (18a)
0.1
0.2
0.5
1
2
5
10
p_s / p^*
XBL6811-7182

Fig. 17

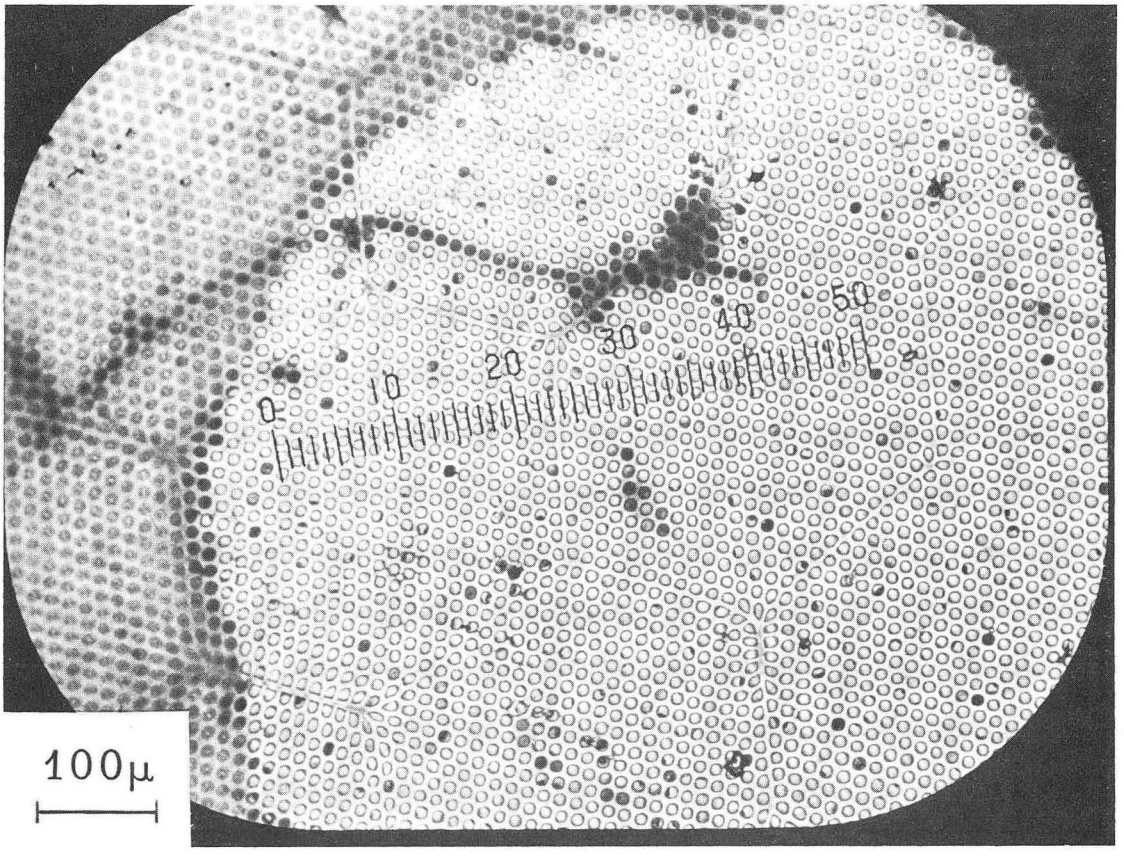

XBB 6811-7096

Fig. 18

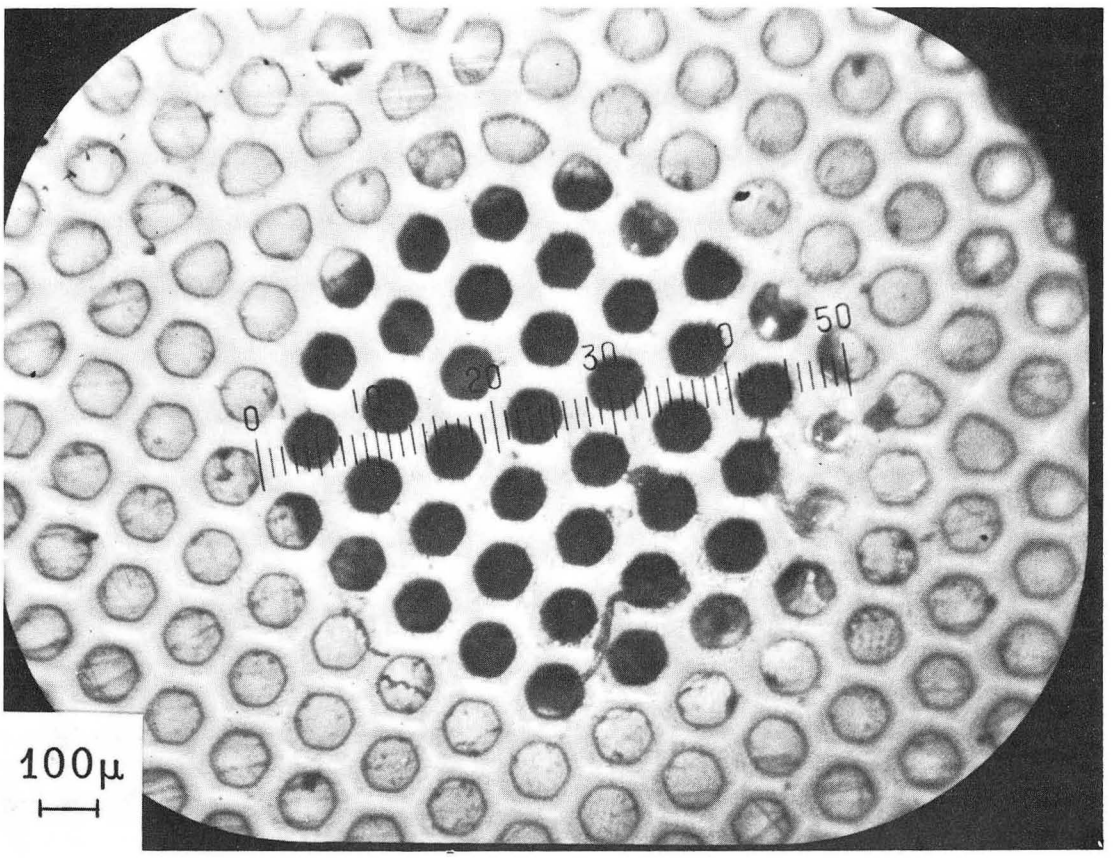

XBB 6811-7097

Fig. 19

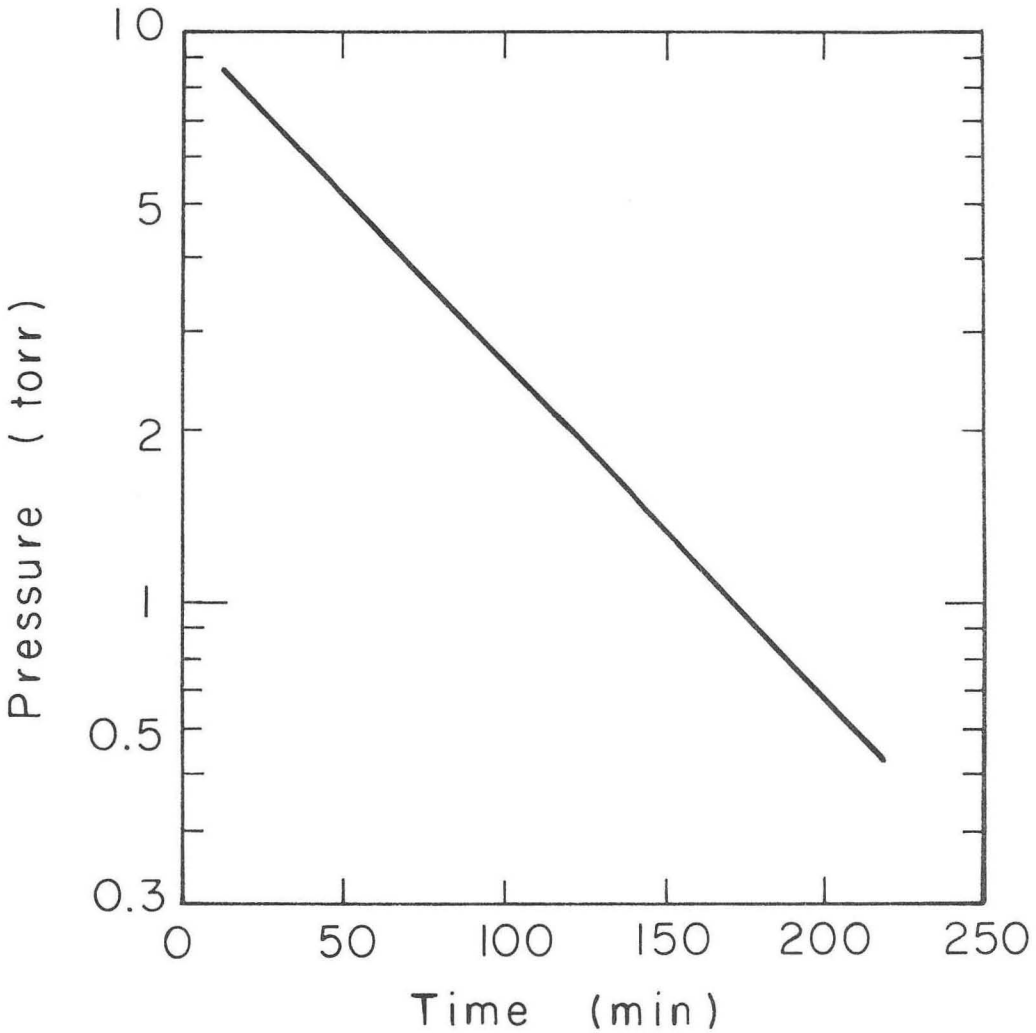

XBL6811-7183

Fig. 20

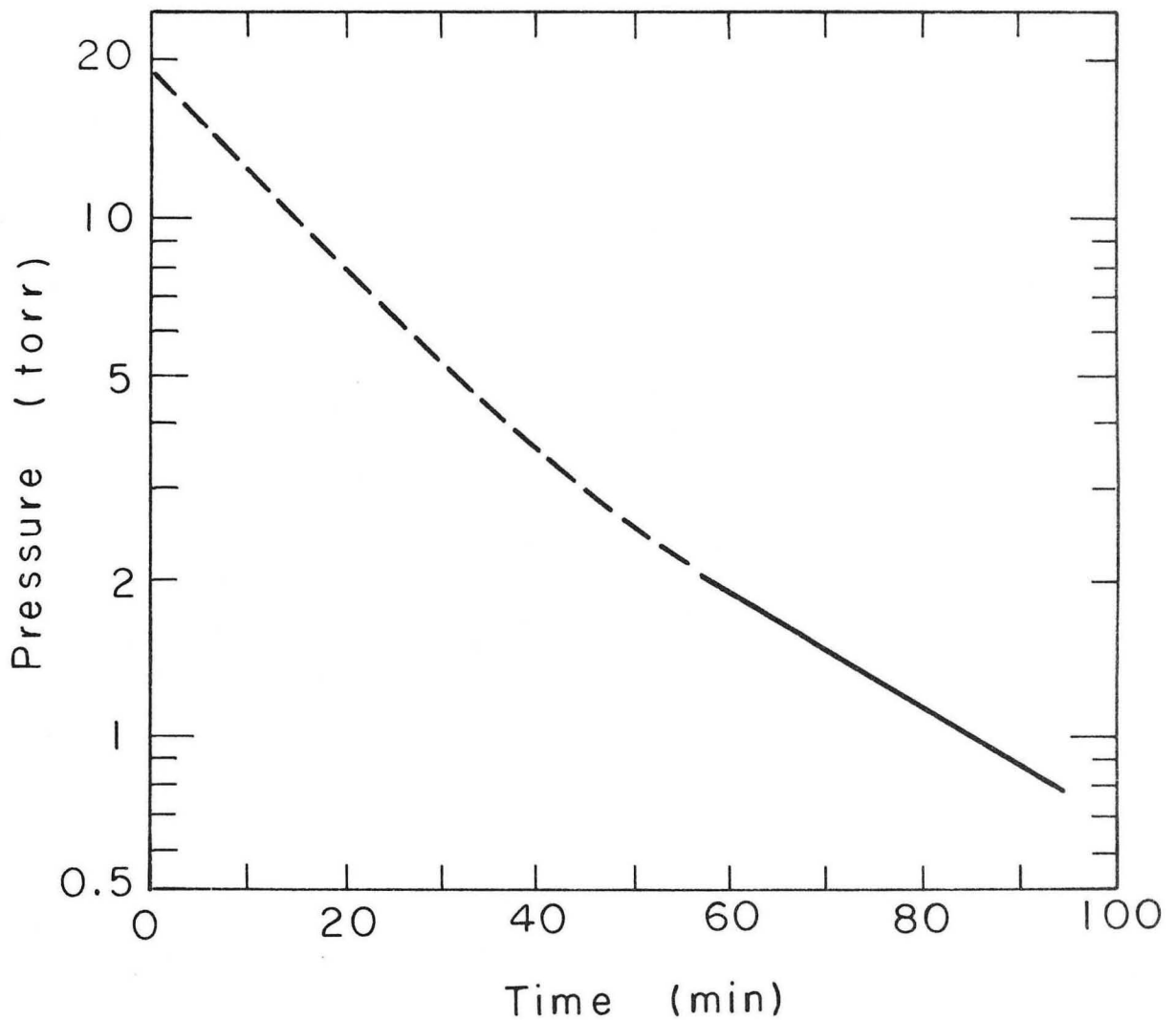

XBL6811-7184

Fig. 21

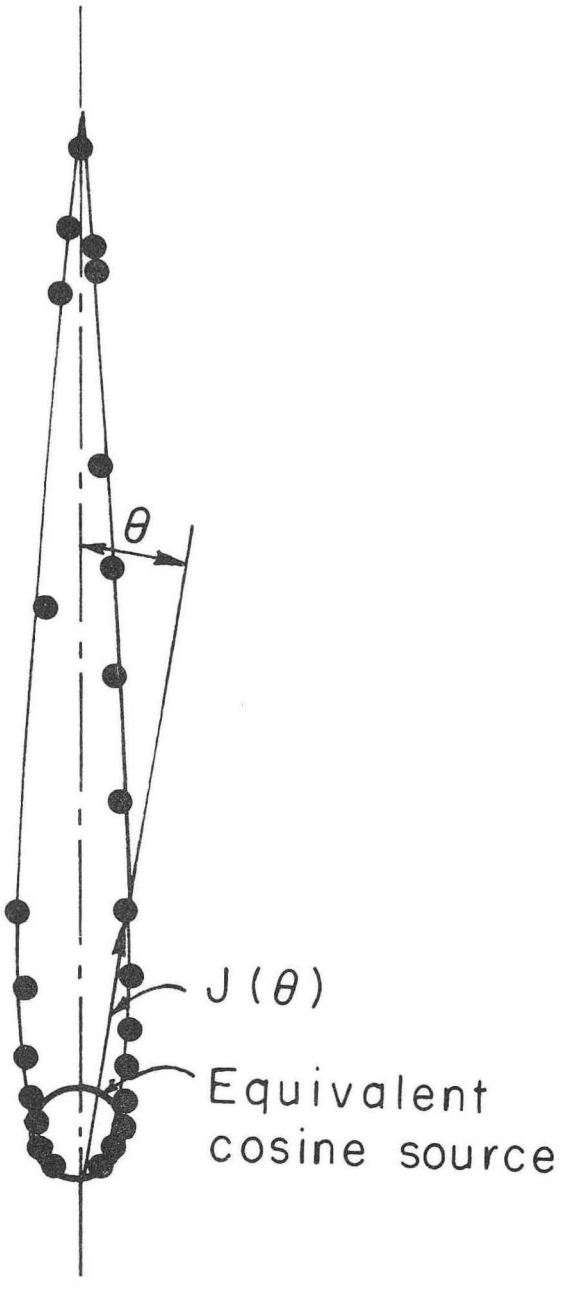

XBL6811-7185

Fig. 22

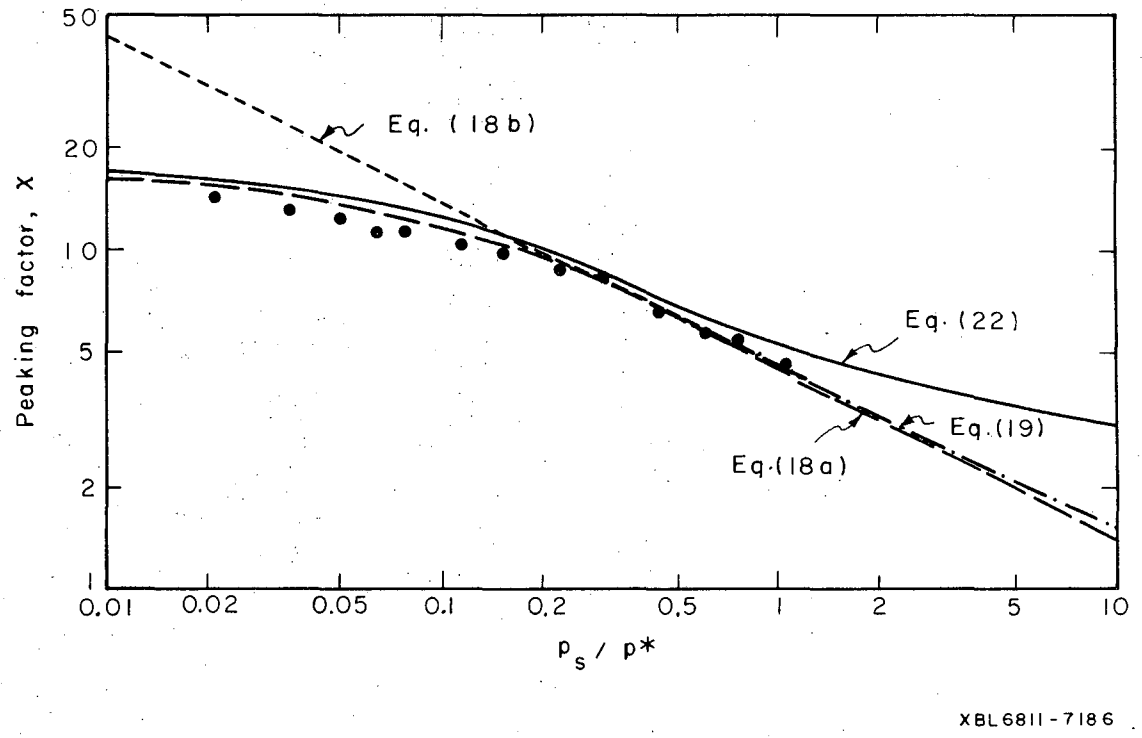
50
20
10
5
2
1
Peaking factor, X
Eq. (18b)
Eq. (22)
Eq. (19)
Eq. (18a)
0.01
0.02
0.05
0.1
0.2
0.5
1
2
5
10
p_s / p^*
XBL6811-7186

Fig. 23

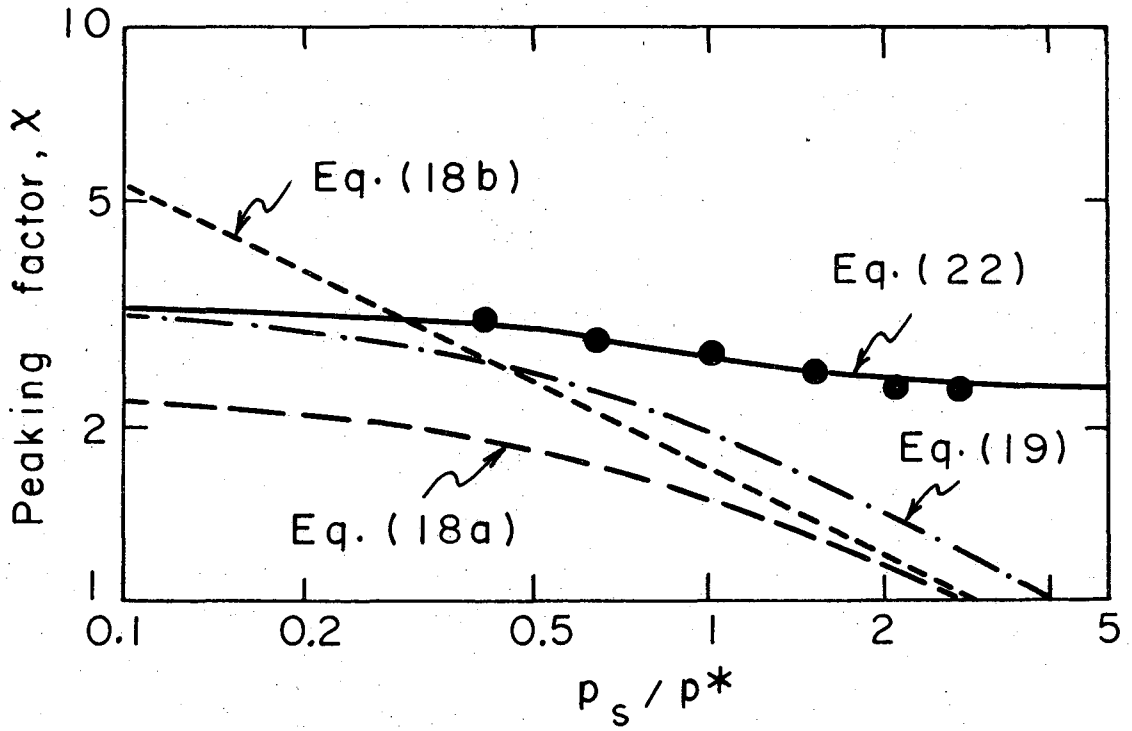

XBL6811-7187

Fig. 24

LEGAL NOTICE

This report was prepared as an account of Government sponsored work. Neither the United States, nor the Commission, nor any person acting on behalf of the Commission:

A. Makes any warranty or representation, expressed or implied, with respect to the accuracy, completeness, or usefulness of the information contained in this report, or that the use of any information, apparatus, method, or process disclosed in this report may not infringe privately owned rights; or

B. Assumes any liabilities with respect to the use of, or for damages resulting from the use of any information, apparatus, method, or process disclosed in this report.

As used in the above, "person acting on behalf of the Commission" includes any employee or contractor of the Commission, or employee of such contractor, to the extent that such employee or contractor of the Commission, or employee of such contractor prepares, disseminates, or provides access to, any information pursuant to his employment or contract with the Commission, or his employment with such contractor.

TECHNICAL INFORMATION DIVISION
LAWRENCE RADIATION LABORATORY
UNIVERSITY OF CALIFORNIA
BERKELEY, CALIFORNIA 94720